Marine and Petroleum Geology 150 (2023) 106154

Contents lists available at ScienceDirect

Marine and Petroleum Geology

journal homepage: www.elsevier.com/locate/marpetgeo

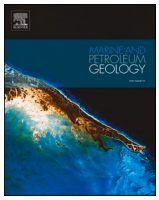

Late Permian-Triassic sedimentary evolution of the Southern Adriatic area based on wells and cores analysis

Mario Borrelli [a,*], Edoardo Perri [a], Michele Morsilli [b], Salvatore Critelli [c]

[a] Dipartimento di Biologia, Ecologia e Scienze Della Terra, Università Della Calabria, Via Pietro Bucci, 87036, Arcavacata di Rende, Cosenza, Italy
[b] Dipartimento di Fisica e Scienze Della Terra, Università di Ferrara, Via G. Saragat 1, 44122, Ferrara, Italy
[c] Dipartimento di Ingegneria Ambientale, Università Della Calabria, Via Pietro Bucci, 87036, Arcavacata di Rende, Cosenza, Italy

ARTICLE INFO

Keywords:
Burano anhydrite
Dolomia principale
Triassic
Paleogeography
Facies analysis
Dolomitization

ABSTRACT

Rock samples from two cores within the Triassic interval of the Puglia 1 well, were studied to reveal the sedimentary facies and diagenesis. The Core 1 (5.048–5.056 m deep) is characterized by laminated dolomudstones with thinly microbial laminae alternated to lenticular/tabular shaped anhydrite crystal levels, suggesting an intertidal/sabkha-type environment. The Core 2 (6.067–6.075 m deep), shows coarse-grained crystalline massive dolomite with remnants of oolites and shell fragments, suggesting a marginal shallow-water setting. Dolomitization is ubiquitous and occurred early after the deposition through the circulation of high saline dolomitizing fluids under general reducing conditions. The early-dolomitization preserved the dolomites from major burial diagenetic transformations, permitting only the ordering and the development of xenotopic textures in the dolomite crystals (aging). Primary anhydrite crystals were lately affected at least by one burial hydration-dehydration cycle, whereas fracture-filling anhydrite is a later-stage diagenetic product of circulating sulphate-rich fluids. Moreover, the integration of Puglia 1 well data with other six exploration wells and a seismic line allowed a possible reconstruction of the Permian-Triassic sedimentary evolution of the Southern Adriatic area. During Permian continental/coastal lagoon settings developed, while in the Ladinian, after a generalized subaerial exposure and an erosional phase, the extensional tectonic inputs linked to Tethys rifting brought to a relative sea-level rise and to the formation of carbonate shelves in NW-SE oriented tectonic depressions. During Carnian-early Norian a further extensional tectonic pulse coupled with a relative sea-level drop, led to the formation of NW-SE elongated intrashelf basin with a consequent enhancement of salinity and settlement of evaporative conditions. This triggered a massive evaporite deposition during the Norian, that filled the basinal areas. Lastly, in the late Norian-Rhaetian a marked relative sea-level rise, restored the connections with open-sea and shifted the evaporite deposition up to the shallowest parts of the basins that previously remained under subaerial conditions.

1. Introduction

The Southern Adriatic Basin is located offshore Italy and Croatia (Fig. 1) in the central Mediterranean sector and represents the innermost portion of the Adria microplate (Vai, 2001; Golonka, 2004; Finetti, 2005; Channell et al., 2022). Since the late Permian to the Early Cretaceous, it experienced an extensional tectonic regime that brought to the opening of the Neo-Tethys Ocean (e.g. Cazzini et al., 2015; Scisciani and Esestime, 2017). Then, since Late Cretaceous, a tectonic inversion occurred as consequence of the collision of African and European plates which, in turn, brought to the development of the two different fold-and-thrust belts systems (Southern Alps, and Dinarides), and later on the Apennine thrust belt (Fig. 1) (e.g. Laubscher and Bernoulli, 1977; Cavazza et al., 2004; Finetti, 2005; Schettino and Turco, 2006; Scisciani and Calamita, 2009; Cazzini et al., 2015).

Such a tectonic puzzle has aroused noticeable interest in the E&P industries that since the 70' acquired numerous seismic reflection profiles and drilled deep wells throughout the entire Adriatic region, leading it to become one of the most significant hydrocarbon provinces of the entire Italian peninsula. It now accounts for the 22% of the total Italian plays with 110 gas-fields and 17 oil-fields (Cazzini et al., 2015). Most of the production is located in the Northern Adriatic (Zone A and B)

* Corresponding author.
E-mail address: mario.borrelli@unical.it (M. Borrelli).

https://doi.org/10.1016/j.marpetgeo.2023.106154
Received 11 August 2022; Received in revised form 27 January 2023; Accepted 31 January 2023
Available online 14 February 2023

involving oil production with the Elsa, Ombrina and Rospo Mare field and also gas production, this latter estimated around 10 billion m^3 per year (Anelli et al., 1996; Lindquist, 1999; Bertello et al., 2010; Casero and Bigi, 2013) (Fig. 1). However, also the Southern Adriatic (north of the Zone F and Zone D), with the Rovesti and Aquila fields, plays an important role for the total Italian gas and oil budget (Fig. 1). In particular, in the Southern Adriatic, a proven fertile source rock is represented by the so-called Late Triassic (Norian-Rhaetian) Burano Anhydrite Fm (Zappaterra, 1994; Caldarelli et al., 2013). In fact, despite the lack of the complete Triassic stratigraphy in this area (with only few wells penetrating the Permian deposits), which not allows to clearly characterize the organic rich facies and a complete Permian-Triassic stratigraphy, the geochemical analyses indicate that the oils found in the Southern Adriatic Basin (e.g. Aquila field) and in the Pre-Apulian zone (NW Greece) are correlated with the late Triassic Burano Anhydrite Formation (Karakitsios and Rigakis, 2007; Caldarelli et al., 2013) and partially to Lower Jurassic anoxic limestones (Emma Limestone -"Calcari Anossici", Caldarelli et al., 2013; Cazzini et al., 2015; Campana et al., 2017; Lipparini et al., 2021).

The Burano Anhydrite Formation and generally the Upper Triassic deposits of the Southern Adriatic Basin, are commonly characterized by alternated carbonate (dolomite)-sulphate deposits (including limited

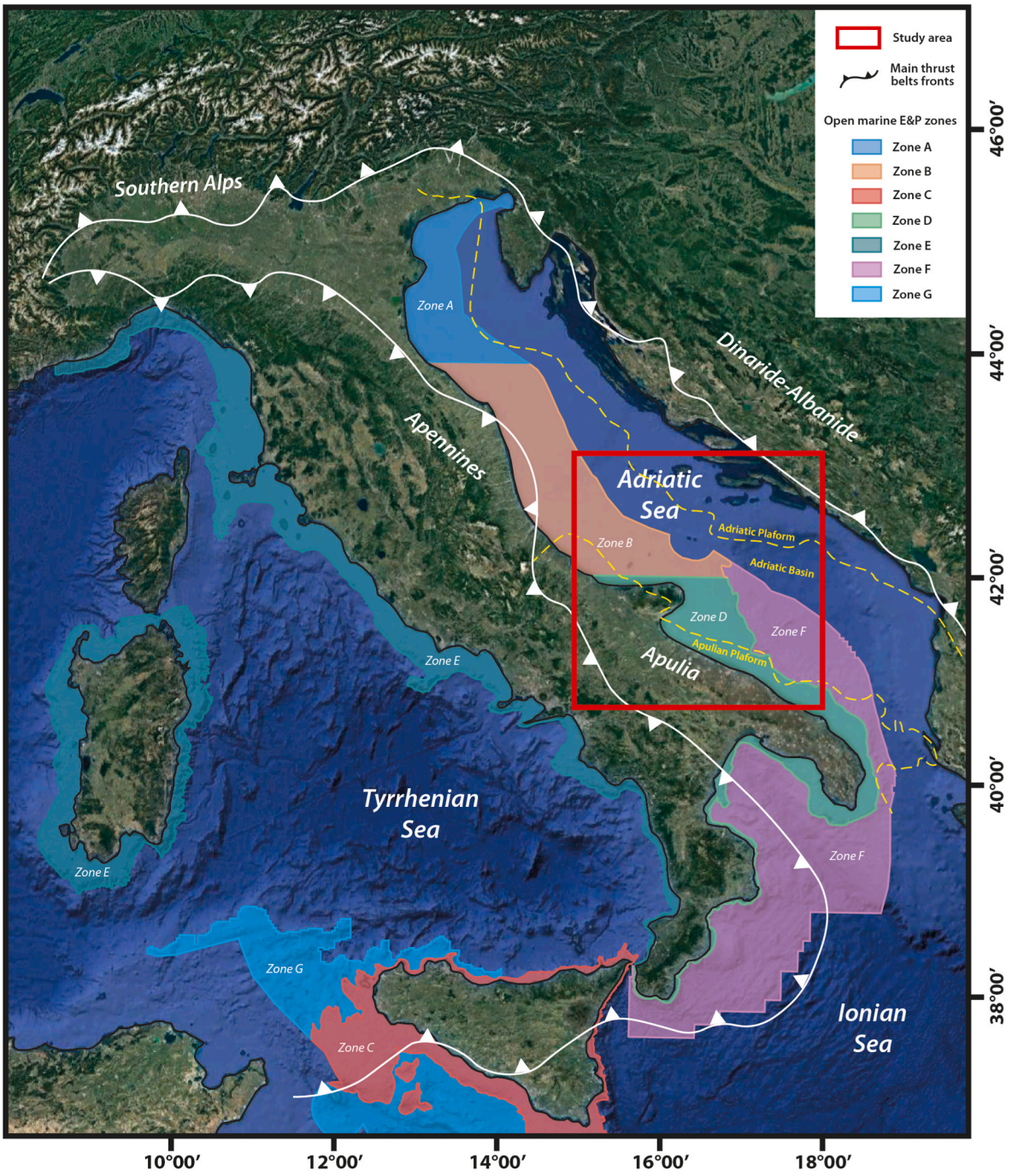

Fig. 1. Location map of the open marine E&P zones of the Italian peninsula in which are highlighted the main Apennines, Southern Alps and Dinarides thrust belts fronts. The Meso-Cenozoic paleogographic position of the Adriatic Basin between the Apulian and Adriatic carbonate platform margins (yellow dashed lines) is shown according to Festa et al. (2014) and Morsilli et al. (2017). E&P data come from the Italian Ministero dello Sviluppo Economico (MISE) (https://unmig.mise.gov.it).

halite) and were firstly characterized by Martinis and Pieri (1964). These deposits are generally found in subsurface and studied through limited well-cores, despite a limited outcrop is also present at Punta delle Pietre Nere in the Gargano Promontory (Bosellini et al., 1999; Morsilli, 2016; Festa et al., 2014) together with spread outcrops in the northern Apeninnes (Lugli, 2001; Lugli et al., 2002). The Burano Anhydrite Formation is generally characterized by alternations of crystalline whitish nodular to chicken wire anhydrites with argillaceous to bituminous shaly laminas and brownish to black thinly crystalline dolomites (e.g. Martinis and Pieri, 1964; Passeri, 1975; Centamore et al., 1986; Ciarapica et al., 1987). These lithological features make the Burano Anhydrite Fm a good source of mineralizing solutions which may greatly influence thermal conductivity changes (and so hydrocarbon generation) through gypsum-anhydrite transition (Jowett et al., 1993; Lugli, 2001) and it can also be used to unravel the ancient paleoclimate and paleogeography with direct implications on the areal extension of the potential producing hydrocarbon sources. Unfortunately, the study of these kind of deposits is extremely complicated and brought, through time, to lots of remarkable discussions because of both the few stratigraphic and sedimentary well-data and the severe post-depositional modifications which generally compromised the products of depositional processes (both carbonate and sulphates). In fact, generally pristine limestones are commonly affected by pervasive dolomitization processes and sulphates experienced multiple gypsum-anhydrite/anhydrite-gypsum transformations depending on the burial and uplift conditions and chemical-physical parameters (e.g. Hardie, 1967; Hardie et al., 1985; Schreiber and El Tabakh, 2000; Testa and Lugli, 2000; Warren, 2006). These diagenetic processes, besides deeply impacting on reservoir heterogeneity, because of the possible significant volume changes (Shearman, 1985), also create a complex array of secondary structures and textures, very commonly masking or completely obliterating the primary ones (Schreiber, 1982; Hardie et al., 1985).

This paper reports for the first time the study of cored samples of both carbonate and sulphate deposits of the late Triassic Burano Anhydrite Fm from Puglia 1 well. Through facies and microfacies analysis, together with mineralogical and isotopic characterization these samples revealed new information regarding the diagenetic history and also the presence of relicts of the original depositional facies. The coupling of these data with the information coming from selected wells in both the on-shore and off-shore Southern Adriatic area together with seismics profile analysis (Fig. 2) could accordingly provide the basis for a renewed definition of the main depositional environments and the paleogeographic configurations of the Adriatic region during the late Permian-Triassic period and also to broadly define the extension of potential hydrocarbon reservoirs in the area.

2. Geologic and stratigraphic framework of the Adriatic domain

The Adriatic region represents the deformed foreland and foredeep

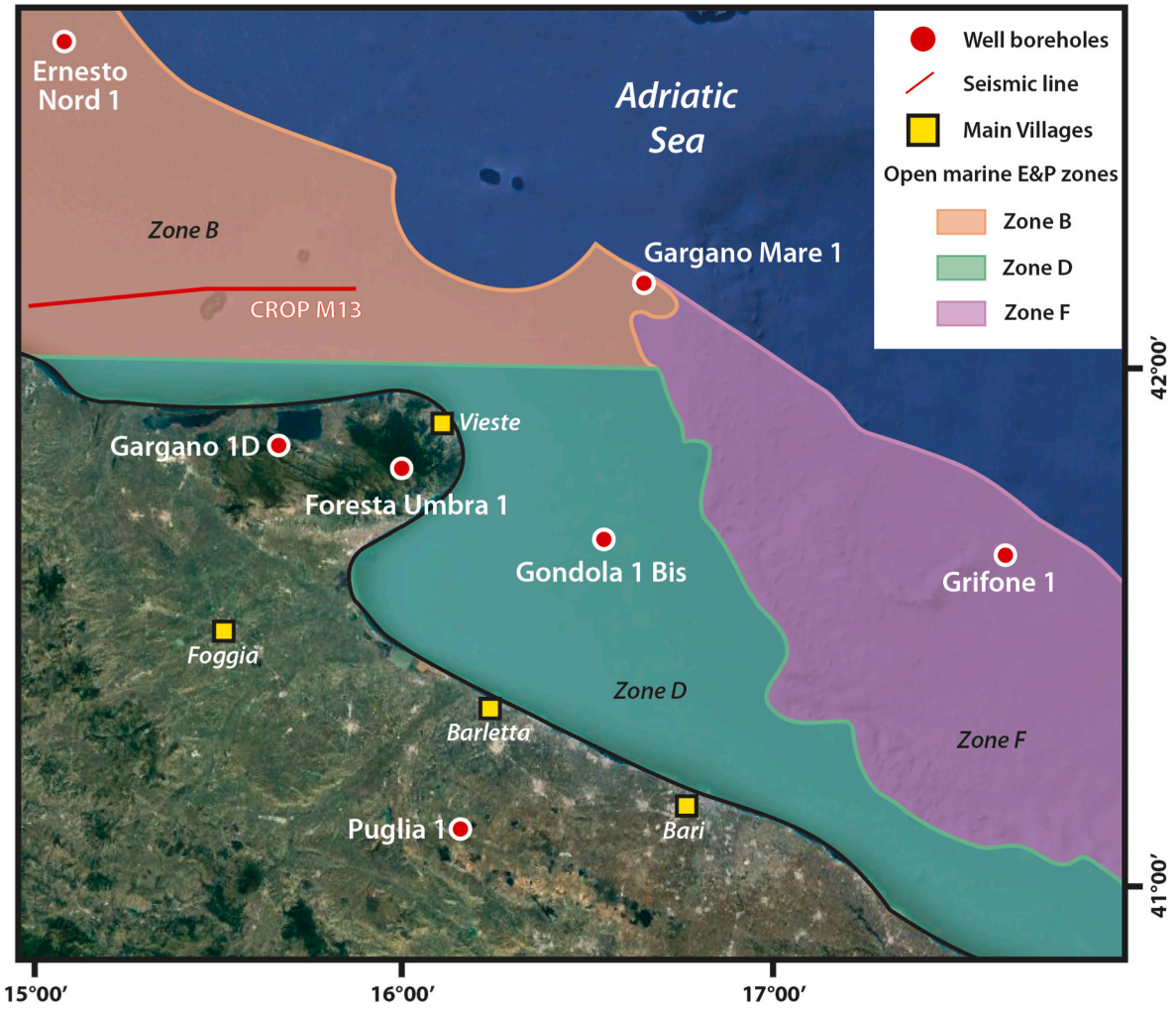

Fig. 2. Geographic location of the selected wells hosting the Burano Anhydrite Fm. Three wells are located onshore whereas the offshore ones are located within three different open marine E&P zones.

of three separate and surrounding fold-and-thrust belts: Apennines, Southern Alps and Dinaride-Albanide systems (Fig. 1) (Battaglia et al., 2004; Piccardi et al., 2011; Casero and Bigi, 2013; Cazzini et al., 2015). In this area, thick deformed sedimentary piles of late Paleozoic to Mesozoic strata, preserving the signature of Tethys rifting phase, are overlain by a Cenozoic succession, mainly composed of sandstones and shales, testifying the successive and still active regional compression and thrust belt activity (Cazzini et al., 2015).

The starting phase of the Tethys rifting can be traced back to the Carboniferous in the present-day Eastern Mediterranean (Al-Belushi et al., 2016; Garzanti and Sciunnach, 1997; Granot, 2016). This oceanic rifting, was generally characterized by a westward progression that reached the nowadays eastern Cimmerian terranes during the early Permian (e.g. Garzanti, 1999; Angiolini et al., 2003, 2007) and the Adriatic and Alpine domain during the Permian-Triassic time (Scisciani and Esestime, 2017). In particular, in these last sectors, the Tethyan rifting promoted a progressive marine ingression that firstly reached the Eastern Southern Alps during the Late Permian, the central Lombardy in the Early Triassic and the Western Alps in the early Anisian (e.g. Bertotti et al., 1993; Manatschal and Bernoulli, 1998; Scisciani and Esestime, 2017). As a consequence, above the Hercynian basement, the sedimentary Late Permian succession of the Italian area was mainly marine (carbonate/siliciclastic) in the central Adriatic (see Chapter 4.1); carbonate/evaporitic in the Dolomites (Bosellini et al., 2003; Stefani et al., 2010; Ronchi et al., 2018) and commonly clastic in the Lombardy and central Alps sectors (Cassinis and Neri, 1992; Virgili et al., 2006; Cassinis and Perotti, 2007; Gretter et al., 2013).

In the early Triassic, the progression of the Tethys rifting brought to the development of NW-SE trending deep extensional basins, such as the Lagonegro and the studied Adriatic Basin (e.g. Scandone, 1975; Laubscher and Bernoulli, 1977; Ciarapica and Passeri, 2002; Iannace and Zamparelli, 2002; Carminati et al., 2013), alternated to terrigenous-carbonate ramps extending up to the Southern Alps sector (e.g. Bosellini et al., 2003; Stefani et al., 2010). Successively, during the late Triassic, the combined effect of the increasing subsidence and sea-level variations (Haq et al., 1988) brought to the development, under general sub-tropical arid climate conditions, of passive margins characterized by a series of carbonate platforms with diffuse shallow-water carbonate deposition (Dolomia Principale Fm of the Dolomites and Alpine sectors) and by wide supra-tidal plains characterized by extensive evaporite deposition (Burano Anhydrite Fm of the Adriatic and Alpine sectors) (e.g. Delfrati et al., 2002; Rigo et al., 2007; Scisciani and Calamita, 2009; Boschetti et al., 2011; Cazzini et al., 2015; Abbas et al., 2018). However, in the end of the Triassic, a marked regional transgression caused the deactivation of most shallow-water carbonate and evaporitic deposition, and prompted a diffused pelagic sedimentation of black shales in the inherited intraplatform basinal throughs (Berra et al., 2010; Cazzini et al., 2015; Wrigley et al., 2015; Scisciani and Esestime, 2017). As consequence, shallow-water carbonate deposition was substantially reduced and confined in limited shelves which persisted during the whole Mesozoic when both extensional tectonic phases (i.e. mid Jurassic) and compressional paleo-inversions (early Cretaceous) occurred (Masetti et al., 2012; Casero and Bigi, 2013; Wrigley et al., 2015; Scisciani and Esestime, 2017).

The passive margin evolution of the Adriatic region ended with the orogenic process responsible for the development of the Alps, Apennines and Dinarides (Faccenna et al., 2003; Doglioni et al., 2006; Patacca et al., 2008; Wrigley et al., 2015). The compressional phase (already since the Late Cretaceous) started with the deformation of the western part of the South Alpine margin (Eo-Alpine phase) and progressed during Paleocene-Eocene with a crustal shortening of the foreland area in front of the Dinaride-Albanide thrust belt (Meso-Alpine phase) in SE Adriatic (Cazzini et al., 2015; Wrigley et al., 2015). In this tectonic scenario, the pre-existing Mesozoic basins and throughs were suddenly filled by turbiditic deposits and the carbonate deposition only persisted during Paleogene-Neogene in limited distal parts of the Dinaric foreland setting (Tamas et al., 2008). Then, the diachronous activation of the Apennine thrust belts (Eocene-Miocene) provoked the progressive segmentation and isolation of multiple and different foredeeps with separate evolutionary histories (Fantoni and Franciosi, 2010; Cazzini et al., 2015). However, a common and generalized Neo-Alpine flexuring triggered the deposition in all these foredeeps of km-thick clastic sedimentary strata (Fantoni et al., 2002, 2004; Fantoni and Franciosi, 2010; Cazzini et al., 2015). This occurred also during the Pliocene-Quaternary with the development of foreland-verging Apennine thrust belt which induced a marked subsidence in front of the Apennine belt, resulting in the deposition of a 7000–8000 m thick foredeep successions (Casero, 2004; Scisciani and Calamita, 2009; Cazzini et al., 2015).

3. Methods

In this work we integrate the well data available from the ViDEPI Project (Visibiltà dei Dati di Esplorazione Petrolifera in Italia), sponsored by MISE (Ministero dello Sviluppo Economico) with the macro- and micro-scale facies and diagenetic characterization of selected key cores.

The ViDEPI dataset includes about 2.305 well data and more than 55.000 km of 2D multichannel reflection seismic profiles acquired along the entire Italian peninsula by different oil companies (mainly Agip) during almost 63 years. For this study an unmigrated seismic profile M13 from the CROP Atlas Project (Scrocca et al., 2003) and a total of 7 wells located in the Southern Adriatic region (Fig. 2) both onshore and offshore in the zone B, D and F were selected for the litho-stratigraphic characterization of the Burano Anhydrite Fm. This stratigraphic unit occurs in all the selected wells at variable depths, always below 1 Km and sometimes exceeding the 6 Km as in the Puglia 1 well. This latter has two recovered cores, one from 5.048 to 5.056 m and the other from 6.067 to 6.075 m, were made available by ENI spa in their laboratories of San Donato Milanese (MI) for the successive facies, mineralogical, stable isotopes and trace elements analysis. For the seismic interpretations we refer to the to the work of Finetti and Del Ben (2005), Scisciani and Calamita (2009), Santantonio et al. (2013), Festa et al. (2014) and Teofilo et al. (2016) which through time defined a "standard" to reliably recognize at large scale various characteristic reflectors even without direct calibration.

A first and preliminary facies description of cores was made at ENI laboratories, which also provided the thin sections of selected intervals subsequently studied using conventional petrographic methods. The bulk mineral composition of all the samples representative of the different sedimentary facies was determined by XRD analyses using a Philips PW1730 diffractometer (Koninklijke Philips N.V., Amsterdam, The Netherlands). Whereas morphological scanning electron microscope (SEM) images were recorded using a FEI-Philips ESEM-FEG Quanta 200 F (Thermo Fisher Scientific, Waltham, MA, USA) at the Università della Calabria. Carbon and oxygen isotope analyses were carried out at the DiSTeM (Dipartimento di Scienze della Terra e del Mare) of the University of Palermo on selected micro-drilled samples of the studied cores, dissolving 8–10 mg of each at 25 °C in 100% orthophosphoric acid for 12 h. Carbon dioxide was obtained by the automated Carbonate Preparation Device Thermo Scientific GasBench II. In view of the different reaction rates of dolomite, the methods proposed by Al-Aasm et al. (1990) were used. The isotopic composition of dolomite is estimated on CO_2 collected after 2 h of reaction at 25 °C; then reaction is continued for 24 h at the same temperature, after which the released CO2 is discarded. Temperature is afterwards increased to 50 °C and the CO_2 produced by the reaction after 4 h is used to determine the isotopic composition of the dolomite. The carbonate isotopic compositions ($\delta^{18}O$ and $\delta^{13}C$) were measured by a Thermo Scientific Delta V Advantage continuous flow isotope ratio mass spectrometer. Results are expressed in delta (δ) notation relative to the Vienna Pee-Dee Belemnite (VPDB) standard. Precision of the carbon and oxygen isotope ratios for duplicate analyses was better than 0.1‰. Mass Spectrometry sensitivity provides

the opportunity to measure isotopic signals even when dolomite is only present as a minor component (<1%).

Lastly, the chemical composition estimation was obtained using a JEOL JXA-8230 electron probe micro-analyzer (EPMA) equipped with five wavelength-dispersive spectrometers (WDS).

4. Results

4.1. Wells and seismic stratigraphy

In the Southern Adriatic area, a total of 7 well logs and the CROP M13 seismic line (Figs. 3 and 4) were studied to define the stratigraphic and syn-sedimentary tectonic architecture of late Permian-Triassic sedimentary succession that generally occurs at very significant depths, always below 1 Km and sometimes exceeding the 6 Km (e.g. Puglia 1 well). For this reason, only two wells (Puglia 1 and Gargano 1D) completely penetrated the Triassic succession up to the Permian, whereas the others are limited to the late Triassic (Fig. 3).

One of the most complete well in terms of general stratigraphy is the Gargano 1D which show a total drilled thickness of 4.850 m, reaching the Permian deposits (Fig. 3). These latter show a thickness of ca. 300 m and are characterized by the presence of mixed clay and carbonate deposits and a basaltic intrusion. An erosive angular unconformity then divides the Permian from the middle to late Triassic succession (Ladinian to Norian-Rhaetian) which shows a total thickness of ca. 3.160 m. At the base of the Triassic succession, the Ladinian deposits are characterized by ca. 160 m of dolomites interlayered with shales levels passing upward into siltstones to sandstones. Upward the late Triassic succession starts with a Carnian-Norian anhydrite dominated body, ca. 700 m in thickness, characterized by crystalline anhydrite generally interlayered with thin dolomite and shaly levels (Fig. 3). The anhydrite dominated body is then overlined by a very thick (ca. 2.300 m) Norian-

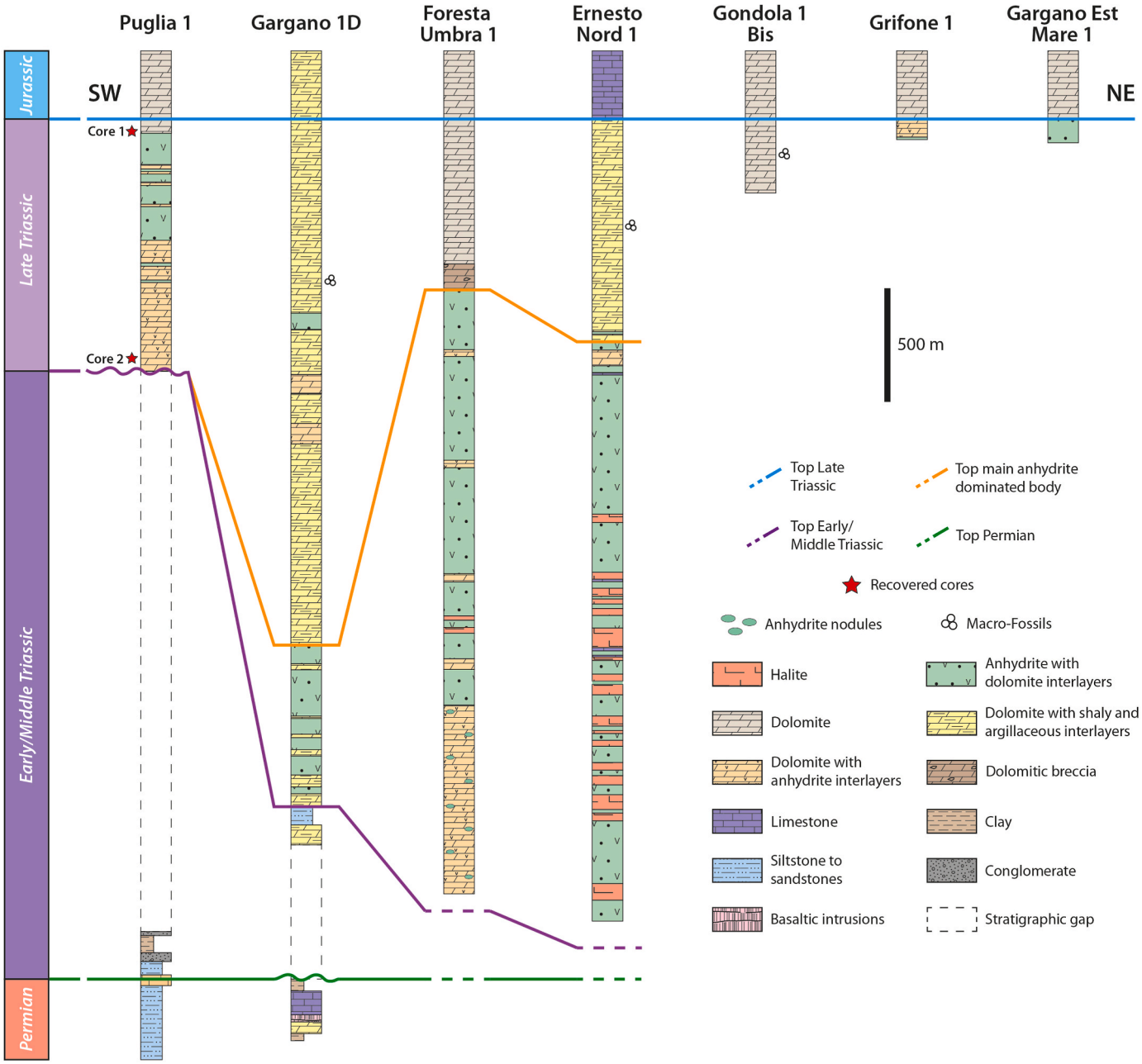

Fig. 3. Permian/Triassic wells stratigraphy and lateral correlations of seven boreholes of the South Apennine and Adriatic areas, located both onshore and offshore. The geographic location of boreholes is reported in Fig. 2. Data from Videpi Project, modified.

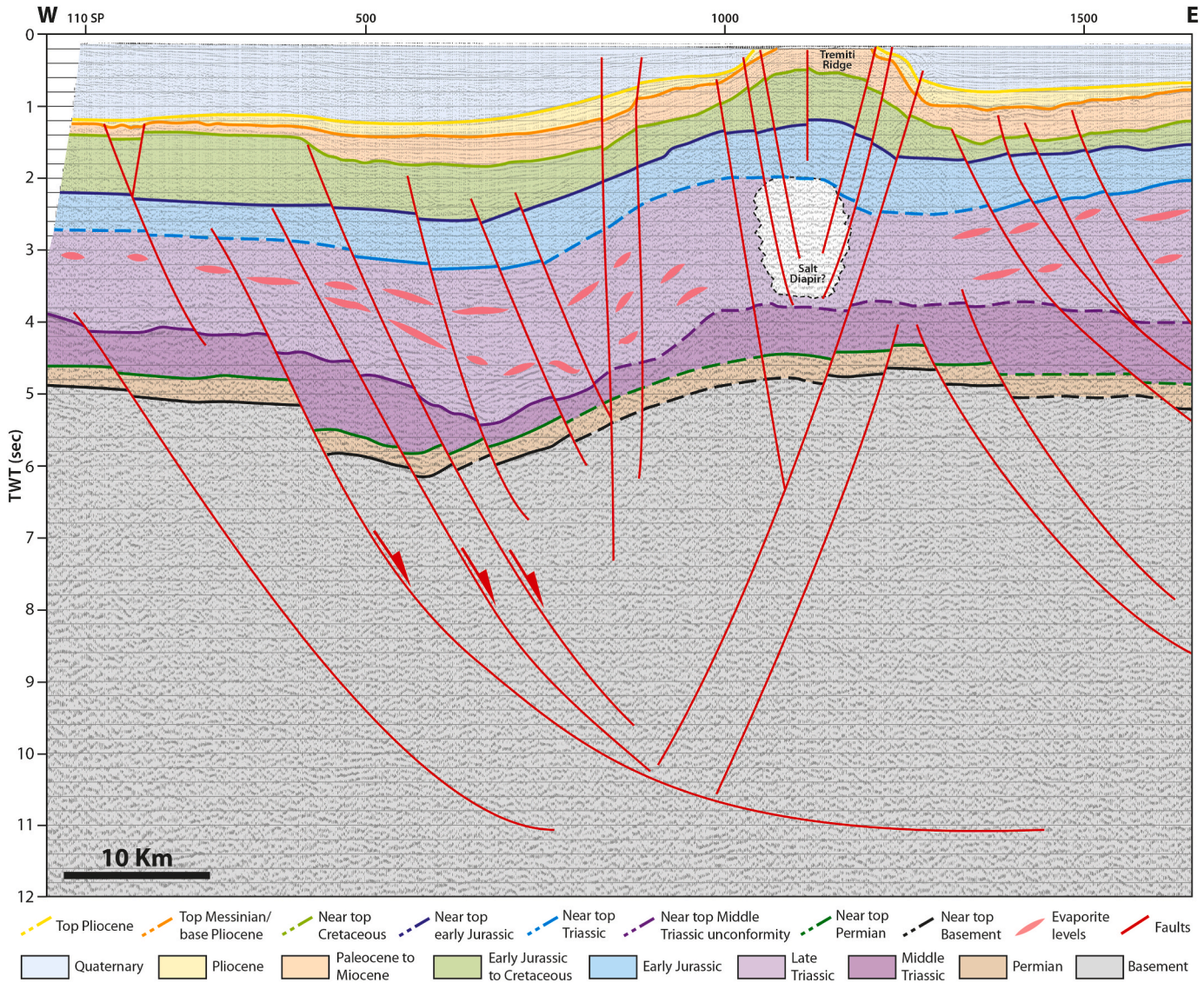

Fig. 4. Interpretation of the seismic reflection profile CROP M13 (stack version) showing the presence of syn-sedimentary Permian?-Triassic E-dipping normal faults which controlled the deposition of the Triassic sedimentary succession. The Central part of the profile shows the presence of a push-up geometry related to Pliocene-Quaternary inversion of the abovementioned normal faults (Scisciani and Calamita, 2009). This tectonic configuration is related to the Tremiti Ridge where a salt diapir is inferred to be present based on the assumption of Festa et al. (2014) and Teofilo et al. (2016). Note the thickness variation of the Triassic succession along the whole seismic profile. Modified after Finetti and Del Ben (2005), Scisciani and Calamita (2009), Festa et al. (2014) and Teofilo et al. (2016).

Rhaetian dolomite dominated body frequently interlayered with argillaceous/shaly levels and sometimes by anhydrite intervals up to 20–40 m thick, which close the Triassic succession (Fig. 3).

The other well reaching the Permian deposits is the Puglia 1, located South of the Gargano 1D well (Fig. 2). It shows a Permian succession mainly dominated by terrigenous deposits of siltstone to sandstones and dolomites with anhydrite interlayers, which passes upward, in stratigraphic continuity, to early Triassic conglomerates and sandstones and rarely dolomites levels (Fig. 3). According to the Eni nomenclature, these early Triassic strata, ca. 200 m in thickness are referred to the Werfen Fm of the Dolomites and Southern Alps (e.g. Stefani et al., 2010). Upward, an erosive surface divides the early Triassic deposits from the late Triassic ones which according to ENI nomenclature correspond to the Burano Anhydrite Fm. These latter show a thickness of ca. 1.100 m and are characterized by dolomite alternated with anhydrite levels, passing upward into fully crystalline anhydrite strata (Fig. 3). In the uppermost part, 50–60 m of very fine dolomite close the Triassic succession (Fig. 3).

The Foresta Umbra 1 and Ernesto Nord 1 are two of the thickest wells in the Southern Adriatic area, since they respectively account for a total drilled thickness of ca. 5.910 m and 6.175 m. However, these wells, located more Nort-Eastward respect to the previous ones (Fig. 2), exclusively penetrate late Triassic deposits of the Burano Anhydrite Fm, according to Eni nomenclature. Both wells are characterized by a stratigraphic architecture similar to the Gargano 1D well, since they both show a late Triassic succession characterized at the base by a main anhydrite dominated body, followed by a dolomite dominated body. In particular, in the Foresta Umbra 1 the main anhydrite dominated body (ca. 2.620 m in thickness) is formed by dolomites alternated to anhydrite levels and frequent anhydrite nodules (ca. 800 m), passing upward into dominant anhydrite strata sometimes showing the presence of halite levels (Fig. 3). Then, the overlying dolomite dominated body (ca. 600 m in thickness) shows at the base a dolomitic breccia passing upward into generally fine dolomites (Fig. 3). Instead, in the Ernesto Nord 1 well, the main anhydrite dominated body shows a thickness of ca. 2.520 m and is typified by the dense alternation of anhydrite and halite strata (Fig. 3). This body is then overlay by the dolomite dominated body (ca. 900 m in thickness), made by dolomite alternated to thin argillaceous to shaly

levels (Fig. 3).

Because of the absence of any unconformities at the top of the Triassic successions of all the studied wells, that indicates a stratigraphic continuity between the Triassic and Jurassic succession (Fig. 3), the late Triassic deposits of the Puglia 1 well, dominantly composed by anhydrite, are laterally correlatable with the uppermost dolomite dominated bodies of the Foresta Umbra 1, Ernesto 1 Nord and also Gargano 1 D (Fig. 3). This implies that the anhydrite dominated bodies of the Foresta Umbra 1, Ernesto 1 Nord and also Gargano 1 D, defined as Burano Anhydrite Fm by ENI nomenclature, are older and consequently not correlatable with the late Triassic deposits of the Puglia 1 well, even if the latter have been ascribed to the Burano Anhydrite Fm by ENI.

The remaining Gondola 1 Bis, Grifone 1 and Gargano Est Mare 1, located eastward in respect to all the previous wells, are less than 500 m in thickness. They consequently show exclusively the uppermost part of the late Triassic succession (Burano Anhydrite Fm according to ENI nomenclature) which is characterized by fractured fine dolomite in the Gondola 1, dolomite and anhydrite alternations in the Grifone 1, and crystalline anhydrite in the Gargano Est Mare 1 (Fig. 3).

The Triassic succession is recognizable in seismic through the E-W oriented CROP M13 line located to the north of the Gargano Promontory (Fig. 2) and interpreted through time by different authors (e.g. Finetti and Del Ben, 2005; Scisciani and Calamita, 2009; Santantonio et al., 2013; Festa et al., 2014; Teofilo et al., 2016; Morsilli et al., 2017) who defined common tectono-stratigraphical features. The seismic line shows the dominant presence of E-NE dipping normal faults, some of which becoming listric at depth and presumably flattening into the lower crust (Finetti and del Ben, 2005; Scisciani and Calamita, 2009). These faults, generally active up to the Jurassic, strongly controlled the thickness of the Permian?-Triassic succession which generally results thicker to E (Fig. 4). A positive flower structure cutting up to the quaternary succession is present in the Eastern part of the line and it identifies the Gargano-Tremiti transcurrent system (Finetti, 1982), where seismic wave diffraction, reflected refractions and velocity distortion phenomena strongly suggest halokinesis of the Triassic evaporites and so the presence of a salt diapir (Festa et al., 2014; Teofilo et al., 2016) (Fig. 4).

The base of the sedimentary cover, above which is present the Permian succession with a constant thickness of circa 0.4 s TWT (Finetti and Del Ben, 2005), is interpreted at circa 5 s TWT in the Western part of the profile and it is downthrown to the east to a maximum depth of circa 6.2 s TWT (Fig. 4). The Triassic succession lies above the Permian interval and is topped by a high amplitude and discontinuous reflector at circa 2.8–3 s TWT (Fig. 4). It is characterized by an eastward thickness variation form circa 2 s TWT to 2.6 s TWT because of the effect of the syn-sedimentary E-dipping listric faults. Within the Triassic succession another high amplitude and generally continuous reflector identifies the top of the middle Triassic unconformity located between 4 and 5.4 s TWT (Fig. 4). This surface highlights an internal thickness variation, especially visible in the middle part of the line and independent from the general tectonic framework, from circa 1–0.8 s TWT up to 0.2 s TWT. The area of minimum thickness of the mid-Triassic succession correspond to the area of maximum thickness of the overlying late Triassic succession, suggesting the presence of a depocenter in this area during late Triassic (Fig. 4). The late Triassic succession is characterized by numerous high amplitude and very discontinuous reflectors, suggesting the presence of evaporitic layers that result very frequent toward the E, up to the positive flower structure where the presence of a diapir is also inferred (Festa et al., 2014; Teofilo et al., 2016). The stratigraphic succession continues with the early Jurassic interval, typified by discontinuous and not very well-defined reflectors but with a constant thickness of about 0.6 s TWT. Its top reflector is located at 2.8 s TWT in the western part of the line, and up to 2 s TWT above the salt diapir in the zone of the Tremiti Ridge (Fig. 4). Upward, the early Jurassic-Cretaceous succession follows and its top is well-highlighted by a package of strong reflectors due to the evaporites of the Gessoso-Solfifera Fm (Teofilo et al., 2016), located between 1.8 s TWT and 0.5 s TWT at the Tremiti Ridge (Fig. 4).

Internally, the early Jurassic-Cretaceous succession is generally typified by well-defined continuous and subparallel reflectors showing an internal thickness variation, inferred as the Apulian Platform depositional profile characterized by an inner platform domain, passing eastward toward a basin. The Paleocene to Miocene and the subsequent Pliocene successions results generally thicker above the inherited depozone of the early Jurassic-Cretaceous body and taper toward the W. In the westernmost part of the line, the top of the Paleocene-Miocene succession is located at 1.4 s TWT, whereas the top of the Pliocene at 1.2 s TWT, both surfaces goes up to the surface along the Tremiti Ridge (Fig. 4). The formation of the Tremiti Ridge can be traced up to late Pliocene and resulted in the formation of a structural high that created depocenters both toward the E and W where the Quaternary succession deposited (Fig. 4).

4.2. Mineralogy, sedimentary facies and petrography of cores

Analyses were based on the characterization of two cores (8 m of thickness each) recovered from the Puglia 1 well (Fig. 3). The Core 1 covers a depth spanning from 5.048 m to 5.056 m, whereas the Core 2 is comprised between 6.067 m and 6.075 m of depth (Fig. 3).

Selected samples of the main lithofacies from both cores were microdrilled and then reduced in powder and analyzed for detecting their mineral composition with X-ray diffraction. XRD spectra revealed the presence, regardless the microfacies, of only two mineral phases: anhydrite and dolomite (Fig. 5).

The dolomite dominated XRD patterns shows the presence of the 101, 015 and 021 reflection peaks (Fig. 5C and D). These latter are the most intense “ordering” reflection which indicate the alternating layers of Mg and Ca. In particular, comparing the intensity of the 110 with the 015 reflections a qualitative indication of the ordering grade can be provided (see Chapter 5.3). In fact, in stoichiometric dolomite the two reflections have nearly similar intensities, whereas with the increasing disorder, the 015 reflection show also decreasing intensities. Generally, the samples coming from the Core 1 (5.048–5.056 m) show a 015 reflection with a lower intensity than the 110 reflection (Fig. 5C). On the contrary, in the samples coming from the Core 2 (6.067–6.075 m) the 015 and 110 reflection show similar intensities (Fig. 5D).

The core between 5.048 m and 5.056 m shows two main lithofacies that appear irregularly alternated in sub-metric layers: laminated bindstones and breccias.

Laminated bindstones are characterized by the alternation of dark to light grayish millimetric flat to crinkly dolomicritic laminae, that form slightly curved packages with, sometimes, small-scale low-relief domes (Fig. 6A and B). This kind of laminations does not show any characters that can be associated to the effect transport currents. This implies their most probably in situ origin as microbial stromatolitic laminae with only small contribute of bound and trapped grains. However, small-scale erosional surfaces can be sometimes observed, along with fine grained clast production and accumulation. Such scattered mm layers appear as wackestones in which can be distinguished dolomicritic sand-sized angular and flat grains with rare bioclasts (Fig. 6C), this time testifying occasional erosional events due to waves or currents. Within the dolomicrite, zones of aggrading neomorphism also occur, with the dolomite microcrystals (circa 8–10 μm in diameter) generally exhibiting a xenotopic texture characterized by anhedral crystals with irregular intercrystalline boundaries (Fig. 6D). Anhydrite crystals are commonly present along laminae as densely packed levels of euhedral to subhedral lenticular and/or tabular mm to sub-mm microcrystal (Fig. 6E). These crystals are generally characterized by nm-scale inclusions (Fig. 6F) and commonly crosscut the lamination surfaces indicating a possible displacive growth.

At the scanning electron microscope, this facies shows the very common presence of residues of organic matter forming μm-size

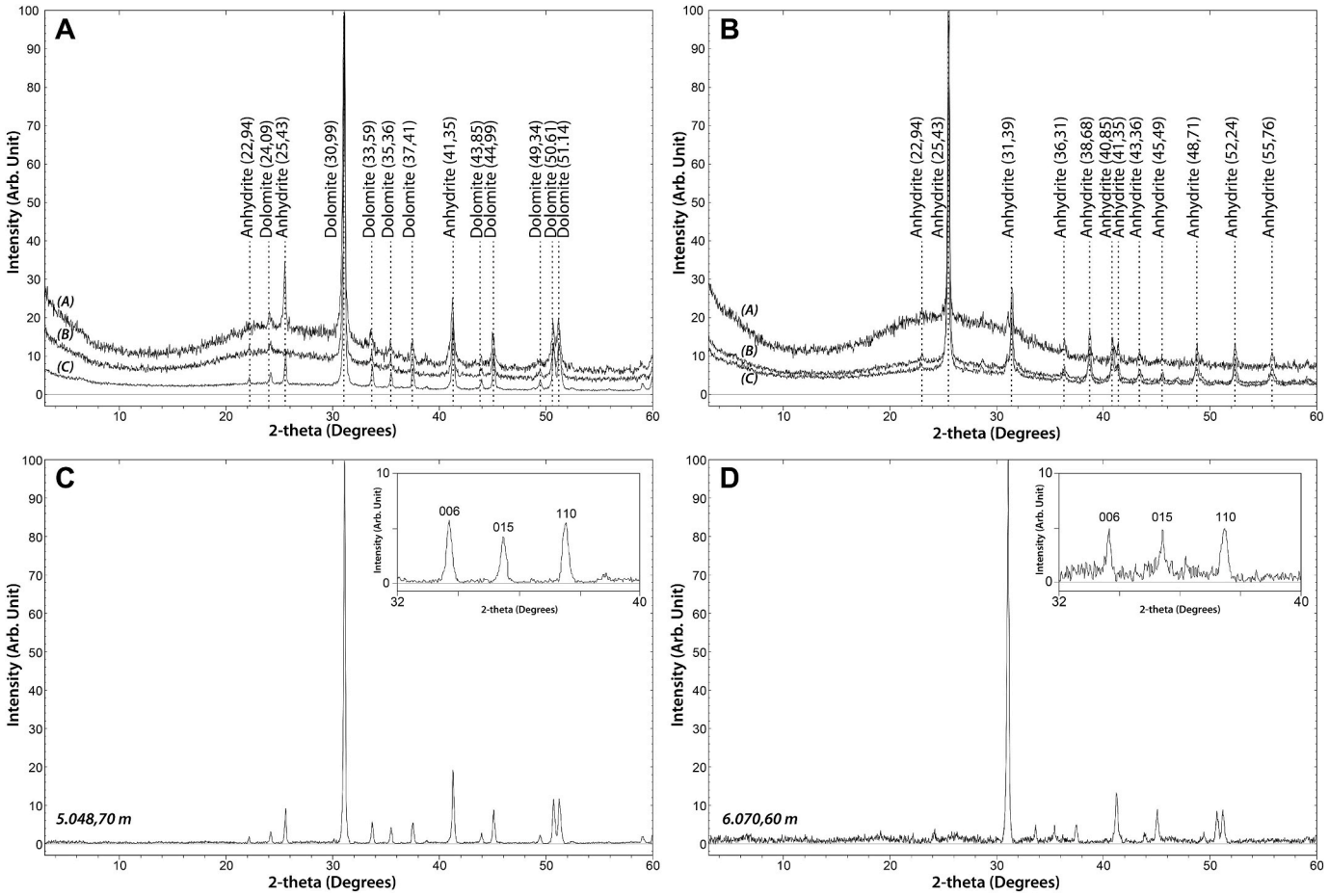

Fig. 5. X-Ray diffraction spectra of 8 selected samples coming from the two recovered cores of the Puglia 1 well. A) The samples 5.048,50 m (a), 6.067,80 m (b) and 5.048,70 m (c) reveal the presence of both anhydrite and dolomite. B) The samples 6.067,40 m (a), 6.072,60 m (b), 5.048,70 m (c) are characterized only by anhydrite. The single X-Ray diffraction pattern of the dolomite dominated samples coming from 5.048,70 m (C) and 6.070,60 m (D) with the magnification of the 006, 015 and 110 reflection peaks is reported.

aggregates in the intercrystalline spaces (Fig. 7A and B). These organic matter aggregates are dominantly characterized by 100 nm-wide spherical (Fig. 7C), and secondarily by elongated curved morphologies (Fig. 7D). Moreover, pyrite framboids are also present (Fig. 7E and F).

Breccia layers are commonly alternated to the laminated bindstones and are generally characterized by angular to sub-angular, millimetric in size, clasts composed exclusively by laminated bindstones (Fig. 8A and B). These breccias are generally clast-supported with the clasts forming a mosaic in which the boundaries fit together, most probably indicating absence of transport, and thus post-depositional brecciation. Clasts are commonly cemented by whitish anhydrite, which also fills the micro-scale (50–100 μm) fractures occurring in both facies (Fig. 8C).

Lastly, stylolites are very common in both facies and, especially in the laminated bindstones, they generally develop parallel to the dolo-micritic laminae (Fig. 8D).

The core between 6.067 m and 6.075 m results generally characterized by light grayish dolomitic breccia with cm-thick dark dolomite clasts (Fig. 9A) and by bioclastic dolo-wackestone showing the presence of ghosts of bivalves shells (Fig. 9B). Bioturbation is very common as highlighted by the presence of cm-wide irregular voids filled by whitish anhydrite cements (Fig. 9C). Both lithofacies are characterized at the microscale by a crystalline closely packed mosaic of anhedral dolomite crystals with a dominant xenotopic texture characterized by curved, lobate and serrated outlines (Fig. 9D). Rarely, hypidiotopic mosaic can also occur. Dolomite crystals are generally equigranular with a size ranging from 100 to 150 μm (Fig. 9E). However, in some portions, inequigranular textures also occur with the coarser crystals measuring 100–150 μm and the finer ones measuring 10–15 μm (Fig. 9F). Both crystal types show at SEM magnification, the presence of generally nanometric cubic voids (Fig. 10A and B). Very commonly the dolomite crystals are zoned with a cloudy dark core and lighter edges sometimes highlighting ghosts of oolite grains (Fig. 10C). Moreover, sometimes dolomitized fragments of bivalve shells can also occur (Fig. 10D). Anhydrite is present exclusively as fracture and void filling, showing lath shape (Fig. 10E) and fibrous radial textures (Fig. 10F).

4.3. Major/trace elements and stable isotopes

For the definition of the chemical composition of the studied rocks two samples were analyzed through WDS: one at 5.048,50 m of depth, representing the laminated bindstones of the Core 1 (5.048–5.056 m), and one at 6.067,80 m representing the crystalline dolostone of the Core 2 (6.067–6.075 m). All the analysis shows nearly constant values of the major elements for both samples and minor variations in the trace elements (Table 1). Generally, the dolomite of both samples results nearly stoichiometric (slightly rich in Ca) with an average of 48.73 mol% of Mg and of 50.85 mol% of Ca.

In the 5.048,50 m sample, dark and light (under optical microscope) dolomicritic laminas that correspond with respectively very fine micritic crystals and coarser micritic to microspar crystals, were analyzed in detail (Fig. 10A). In average both laminae types are typified by 50,72 mol% of Ca, 48,74 mol% of Mg, 2.139 ppm of Na, 318 ppm of Sr, 211 ppm of Fe and 119 ppm of Mn. However, the dark lamina is characterized by slightly higher values of Na and Sr (2.250 ppm and 370 ppm

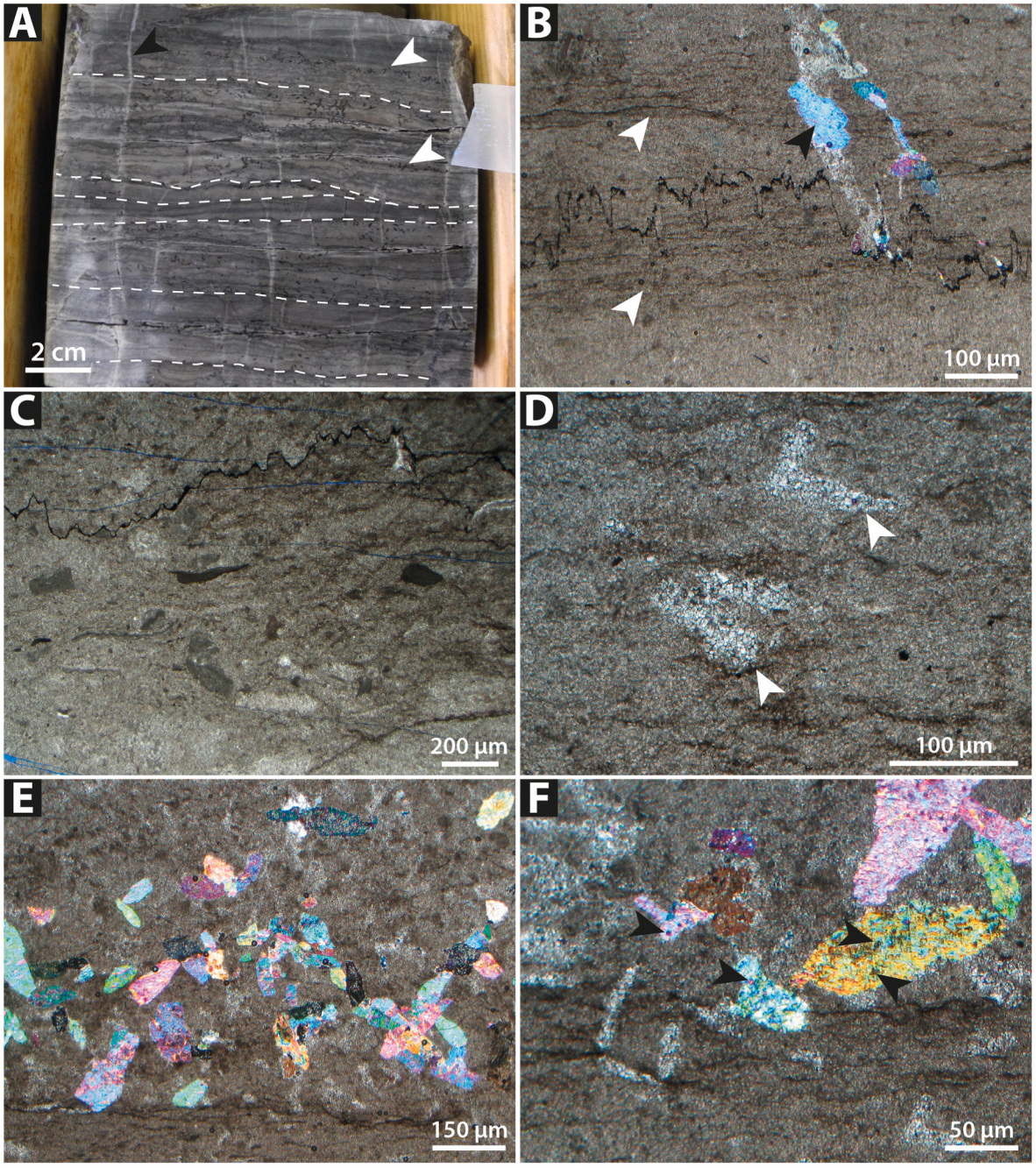

Fig. 6. A) Polished surface of the Core 1 (5.048 m–5.056 m) showing mm flat to crinkly dark to light grayish laminas (dashed white lines) with densely packed anhydrite crystal levels (white arrows). Sometimes serrated fractures, perpendicular to the laminas and cemented by whitish anhydrite (black arrow) also occur. B) Microscale view of the planar to crinkly laminas (white arrows) of the laminated bindstones, anhydrite crystals are also present (black arrow). C) Level with disorganized flattened dolomicritic clasts. D) Area of aggrading neomorphism (white arrows) with the coarser dolomite crystals showing a xenotopic texture. E) Level of euhedral to subhedral lenticular and/or tabular mm to sub-mm anhydrite crystals. F) Magnification of anhydrite crystals with internal inclusions (black arrows).

respectively), whereas the light lamina shows higher values of Fe and Mn (271 ppm and 138 ppm respectively) (Table 1).

In the 6.067,80 m sample, a coarse (150 µm in diameter) and clear anhedral dolomite crystal and two zoned dolomite crystals (circa 130–150 µm in diameter each) were analyzed (Fig. 11A and B). In average all these dolomite crystals are characterized by 50,92 mol% of Ca, 48,72 mol% of Mg, 2.162 ppm of Na, 126 ppm of Sr, 1158 ppm of Fe and 108 ppm of Mn. In detail, the coarse dolomite crystal results characterized by the highest mol% of Ca of the entire dataset (51.18%) and lowest value of mol% of Mg (48.59%). In addition, it results abundant in Sr (240 ppm) and deficient in Na (1.671 ppm), Fe (307 ppm) and Mn (86 ppm), in respect to the zoned dolomite crystals of the 6.067,80 m sample (Table 1). In fact, the zoned dolomite crystals show the highest Fe values of the entire dataset (2.003 ppm and 1.165 ppm), and values of Na (2646 ppm and 2169 ppm) and Mn (100 ppm and 140 ppm) higher than the coarse dolomite crystal and similar to the dark and light dolomicritic laminae of the 5.048,50 m sample (Table 1).

The stable isotopes' analysis was performed on the dolomites of both the 5.048–5.056 m and 6.067–6.075 m cores (Fig. 12). In particular, the 5.048–5.056 m is characterized by a relatively wide range of $\delta^{13}C$ values spanning from 1.55‰ to 2.31‰ and by $\delta^{18}O$ comprised between −2‰ and −3.89‰. Whereas the 6.067–6.075 m core is characterized by a

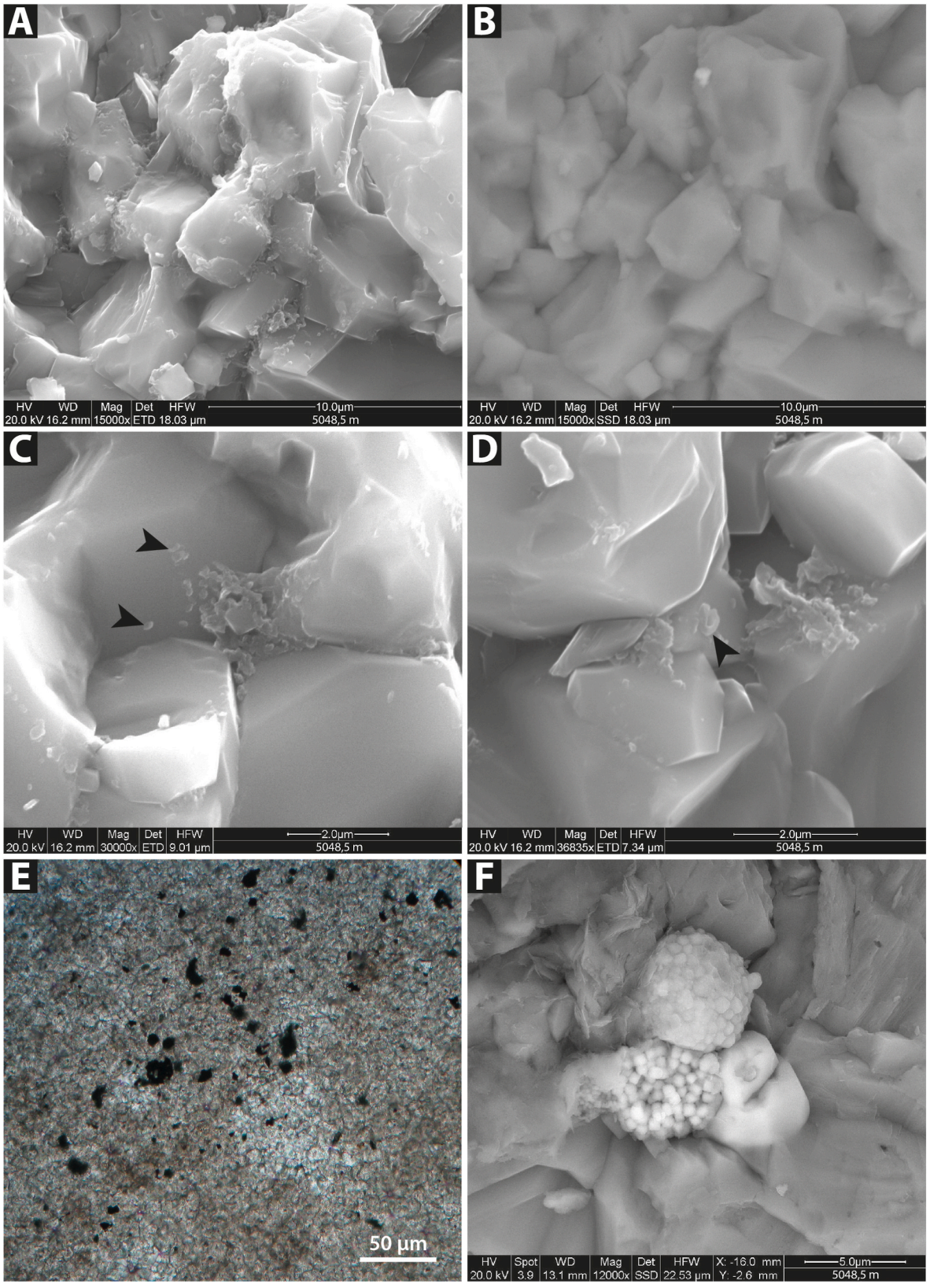

Fig. 7. Secondary electrons (A) and backscattered (B) SEM images of aggregates of organic matter (transparent in the backscattered view) within the intercrystalline space of the laminated bindstones. The organic matter appears dominantly characterized by nm spherical morphologies (C) and secondarily by curved tubular morphologies (D) (black arrows). Thin section (E) and SEM Secondary electrons (F) views of pyrite which commonly assumes a framboid package (F).

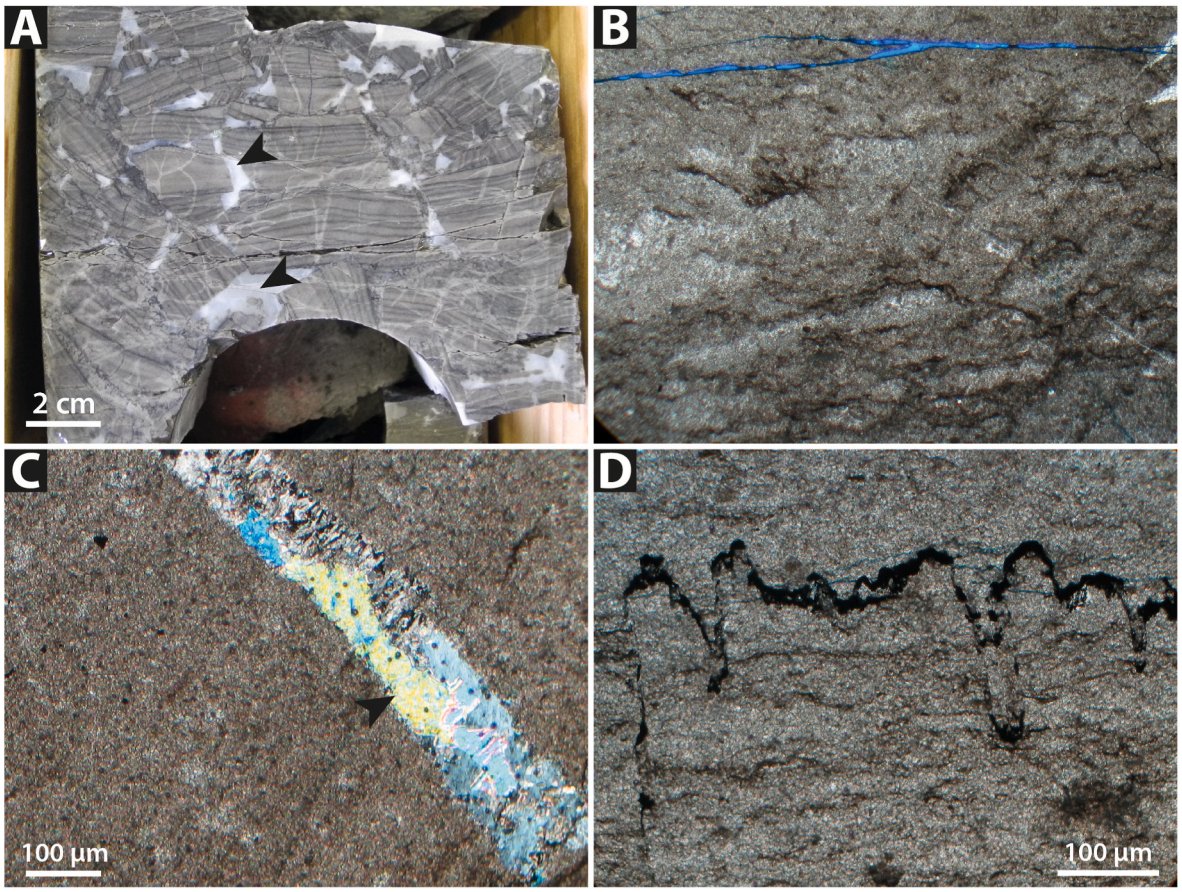

Fig. 8. A) Polished surface of the Core 1 (5.048 m–5.056 m) showing a clast-supported breccia characterized by angular to sub-angular (sand to conglomerate-size) clasts composed exclusively by laminated bindstones. The matrix is represented by whitish anhydrite filling cement (black arrows). B) Thin section view of one of the breccia clasts, showing the typical look of the laminated bindstones (see also Fig. 5B). C) *Fracture filled by clear anhydrite (black arrow). D) Example of a stylolite that commonly occur in both the breccia and laminated bindstones facies. Note its development parallel to the dark dolomicrite laminas.*

very narrow range of $\delta^{13}C$ values, varying from 1.27‰ to 1.57‰ and by a $\delta^{18}O$ spanning from −2.22‰ and −4.2‰.

5. Discussion

5.1. Sedimentary environment

Despite the strong diagenetic alteration of the analyzed samples (see chapter 5.3), remains of the original fabrics and textures of the deposits are still preserved, and can be used to infer the original sedimentary environment of deposition. In the Core 1 of the Puglia 1 well (5.048–5.056 m) can be seen the presence, both at macro- and micro-scale (Fig. 6), of thin levels rich of lenticular and tabular anhydrite crystals interlayered with dolomicritic laminae (Fig. 6E and F) which are interpreted as microbial stromatolitic bindstone. This kind of facies also typifies modern-time peritidal marine environments such as sub-tropical sabkha settings (e.g. Aref and Taj, 2018; Manaa and Aref, 2022). There, microbial mats flourish in enhanced aridity and high salinity and, thanks to the microbial metabolic activity, bio-mediate the precipitation of carbonate minerals (e.g. Vasconcelos et al., 2006; Bontognali et al., 2010; Perri et al., 2018). In the same mat, evaporitic crystals, generally abiotic, are also formed as displacive gypsum lenses frequently forming sulphate dominated mm-thick levels, often associated with less frequent halite (e.g. Aref and Taj, 2018), very similar to those observed in the studied samples (Fig. 6E and F). In some cases, evaporitic minerals can be very pervasive in the microbial deposits, forming thick layers inter-bedded with microbialites which can be easily dissolved by freshwater influxes related to prolonged subaerial exposure (e.g. Borrelli et al., 2021). If the dissolution process results very effective, the collapse of the cemented bindstones occur and the formation of in situ carbonate breccias may take place. As consequence these breccias are formed by clasts of the same composition as the original deposit, with the lack of any evidence of physical transport (Fig. 8A) (e.g. Pedley and Grasso, 1993; Rouchy and Caruso, 2006; Caruso et al., 2015, 2016; Gindre-Chanu et al., 2020; Borrelli et al., 2021).

For what concerns the studied sulphate minerals, they are now represented by anhydrite. The anhydrite crystals in the microbial bindstones generally show corroded borders and lots of inclusions in the crystal cores (Fig. 6F). These latter testify at least one cycle of dehydration–hydration and so gypsum-anhydrite transformation. In fact, sulphates are highly susceptible to diagenetic processes (e.g. Hardie et al., 1985; Schreiber and Tabakh, 2000) and the transformation from gypsum to anhydrite and *vice versa* can occur multiple times depending on the burial and uplift conditions, complicating also the definition of the original depositional mineral (e.g. Testa and Lugli, 2000). Based exclusively on the crystal morphology is consequently not possible to determine if the sulphate crystals firstly precipitated as gypsum or as anhydrite. In any case, this does not affect the depositional interpretation since in modern intertidal to supratidal sabkha environments, gypsum crystals show an identical macro- and micro-scopic morphology whether they are primary or formed by early-hydration of anhydrite nodules (El-Tabakh et al., 1997, 1998; Schreiber and Tabakh, 2000).

In the Core 2 of the Puglia 1 well (6.067–6.075 m) diagenesis (mainly dolomitization) destructed almost totally the primary textures and fabric, making extremely difficult to define the original depositional facies and the proposed interpretation can consequently result highly

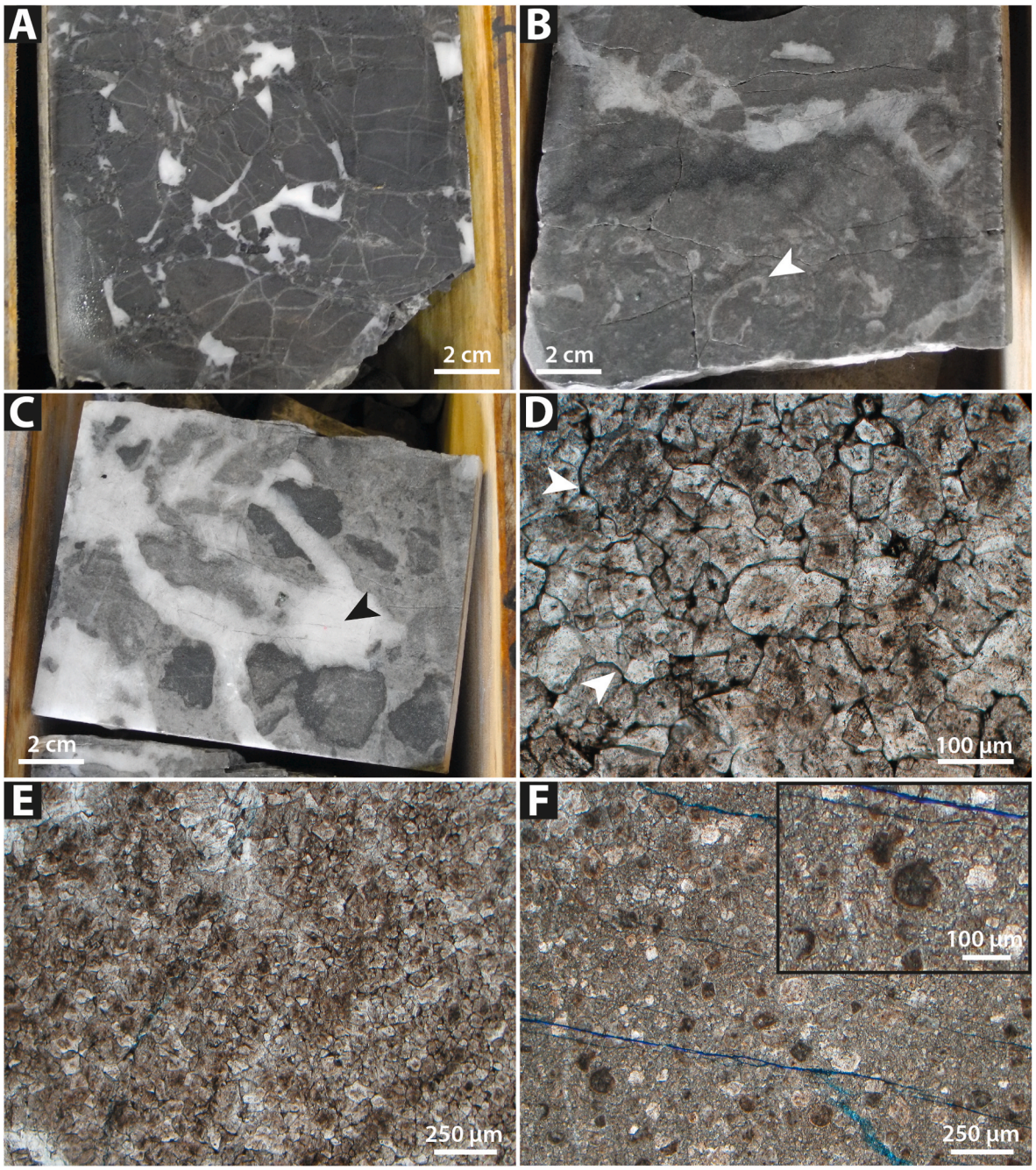

Fig. 9. A) Polished surface of the Core 2 (6.067 m–6.075 m) showing a breccia layer with dark grey dolomite clasts cemented by whitish crystalline anhydrite. B) In some part of the Core 2 (6.067–6.075 m) bioclastic dolowackestone occur. They show the presence of recrystallized bivalves shells (white arrow). C) light grayish dolomitic breccia with dark grayish dolomite clasts. This facies is characterized by large bioturbation voids filled by whitish anhydrite cement (black arrow) (6.067–6.075 m). D) Xenotopic texture characterized by closely packed anhedral dolomite crystals with mostly curved (white arrows), lobate and serrated irregular intercrystalline boundaries. E) Crystalline dolomite with equigranular texture of the dolomite crystals ranging in size from 70 to 100 µm. F) Inequigranular texture of the crystalline dolomite with the coarser subhedral dolomite crystals measuring 70–100 µm and the finer xenotopic dolomite measuring 10–15 µm. A magnification of the xenotopic microcrystals and the subhedral dolomite crystals is also reported.

speculative. However, both at macro- and micro-scale, ghosts of primary depositional features can be sometimes showed. Particularly, in the analyzed samples, at the macro-scale is possible to find out the presence of breccias and bioturbated levels associated to bioclastic dolowackestones (Fig. 9A, B, C); whereas at the microscale, within a massive crystalline dolomite xenotopic mosaic, relicts of disarticulated bivalve shells and probably ghosts of oolites occur (Fig. 10C, D). The presence of these features leans towards a more open marine environment with an enhanced hydro-dynamism that can in turn erode, transport and accumulate carbonate clasts, shells and also form oolites. However, the presence of dolowackestone levels (Fig. 9B) also indicates that the high energy condition was not continuous, and so interrupted by moments of relatively low energy. These environmental conditions can be generally compatible with a trasitional inner platform to margin setting (e.g. beach, shoals and/or lagoon environments) commonly characterized by: 1) the intermittent effect of high energy oscillatory flows of fair weather and storm waves and related currents, which can actively erode previously deposited sediments and form breccia deposits (tempestites),

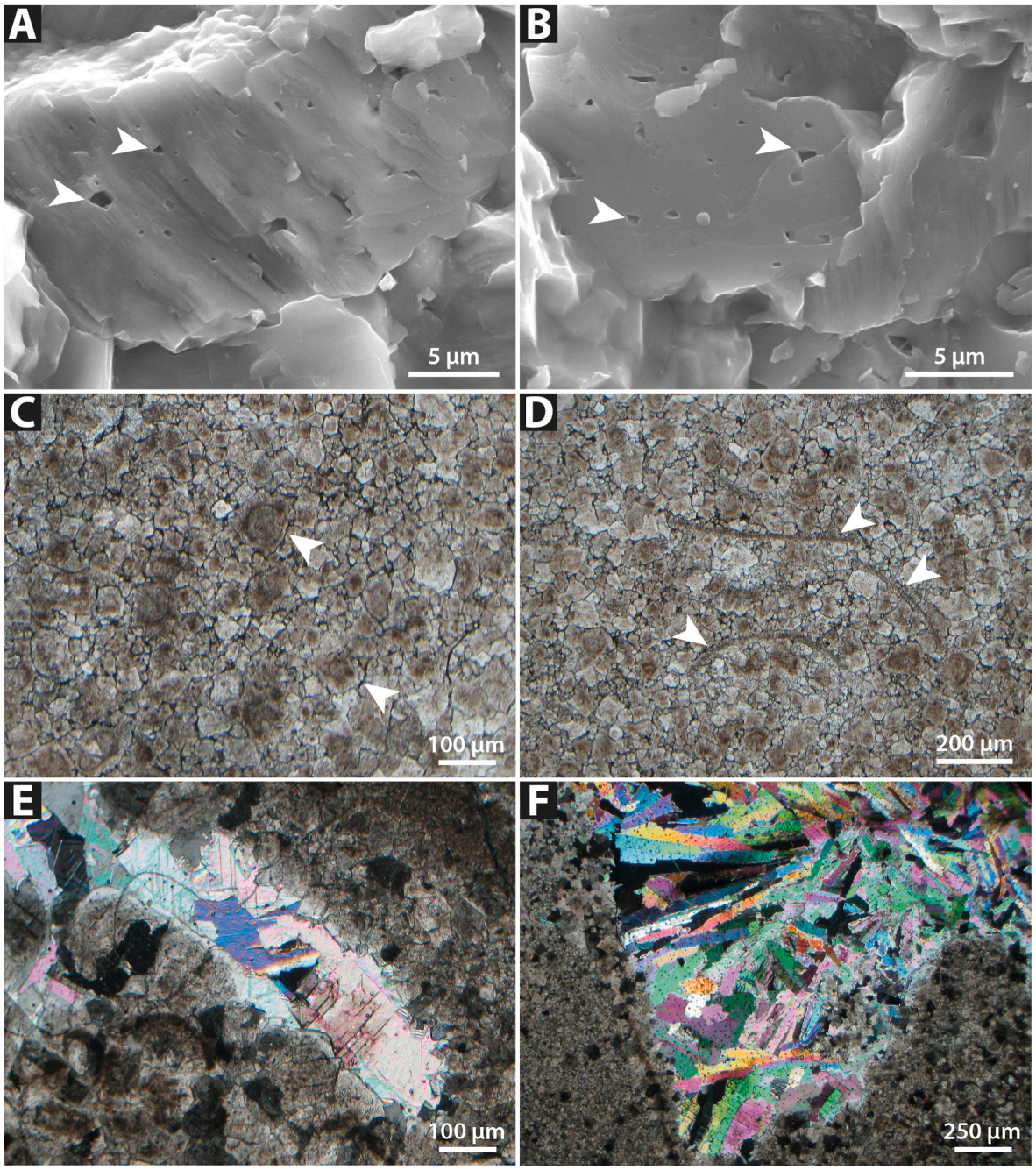

Fig. 10. Secondary electron SEM images (A, B) showing dolomite crystals with sparse cubic to prismatic voids (white arrows). C) Zoned dolomite crystals (white arrows) with cloudy dark core and lighter edges highlighting ghosts of oolite grains. D) Dolomitized bivalve shells fragments (white arrows). Lath shaped (E) and Fibrous radial (F) void-filling anhydrite.

transport bioclasts and form oolites that can also accumulate to form shoals or dunes (e.g. Cruz and Eberli, 2019; Harris and Purkis, 2019); 2) by periods of quiet, that permit the deposition of suspended muddy sediment, establishing also better conditions for the grazing and feeding of various benthonic organisms that can cause the bioturbation (e.g. Pemberton and Wightman, 1992; Clifton, 2006).

5.2. Diagenesis

The characterization of the diagenetic history of the Burano Anhydrite Fm in the Southern Adriatic area can results very challenging because of the few outcropping rocks and the rarity of cores. The study of the two recovered cores from the Puglia 1 well (Fig. 3) gave the opportunity to constrain the main diagenetic processes occurred to the Norian Burano anhydrite dominated body, highlighting the ubiquity of dolomitization process in both Core 1 (5.048–5.056 m) and Core 2 (6.067–6.075 m) with some differences.

The Core 1 is characterized by the retention of the original depositional fabric of laminated microbial bindstones and dolomudstone-dolowackestones commonly associated to anhydrite-rich levels. The presence of fabric-retentive dolomites can generally suggest an early-stage of pervasive dolomitization at near-surface conditions (e.g. Berra et al., 2020). This process is consistent with a sabkha-like dolomitization model (e.g. Tucker and Wright, 1990; Warren, 2000; Meister et al., 2013) - that is the inferred depositional environment rich of evaporites for the studied deposits (see Chapter 5.1) - and is supported by the

Table 1
Major (Ca and Mg mol%) and trace elements (Na, Sr, Fe, Mn mol ppm) of the dolomite in the 5.048,50 sample and 6.067,80 sample.

	mol (%)		mol (ppm)			
	Ca	Mg	Sr	Na	Fe	Mn
5048,50 dark dolomicrite lamina	50,03	49,10	558	3911	88	0
	50,71	48,86	125	2119	356	380
	50,80	48,71	820	2398	247	323
	50,69	48,75	998	1965	0	54
	50,57	49,00	193	1992	0	0
	50,37	49,24	0	2283	0	0
	50,84	48,92	234	680	559	0
	50,70	48,66	1175	2218	0	0
	50,72	48,81	0	1992	303	435
	50,61	48,92	321	2064	0	0
	50,73	48,77	0	3117	0	0
	50,77	48,77	11	2266	246	0
Average	50,63	48,88	370	2250	150	99
5048,50 light dolomicrite lamina	50,55	48,86	344	2455	906	283
	50,38	49,41	0	631	0	194
	50,88	48,76	234	1316	0	0
	50,77	48,79	0	1935	0	0
	50,82	48,58	321	1729	816	388
	50,37	48,10	1104	2433	0	0
	51,30	48,13	0	1735	595	225
	50,96	48,10	246	2127	420	285
	51,01	48,27	686	2958	0	0
	51,15	48,44	667	1779	0	160
	51,65	48,03	0	1755	0	122
	50,35	49,32	0	1916	0	125
	50,60	48,69	0	3460	0	0
	50,51	49,00	0	2572	0	424
	50,90	48,60	0	2539	857	0
	50,94	48,66	666	1101	749	0
Average	50,82	48,61	267	2028	271	138

	mol (%)		mol (ppm)			
	Ca	Mg	Sr	Na	Fe	Mn
6067,80 coarse dolomite crystal	51,93	47,91	0	1611	0	0
	50,09	49,33	749	5073	0	18
	50,28	49,51	954	909	214	91
	51,07	48,75	0	1805	54	0
	51,83	47,96	139	1416	528	0
	51,56	48,36	0	704	0	129
	52,01	47,85	116	354	1003	0
	51,21	48,59	437	1401	162	37
	51,14	48,69	0	1352	377	0
	50,74	48,92	0	2084	733	581
Average	51,18	48,59	240	1671	307	86
6067,80 zoned dolomite crystal	50,47	48,77	465	3281	3887	0
	50,36	49,39	0	1137	954	421
	50,86	48,40	336	4108	2873	0
	50,79	48,92	0	2379	399	55
	51,33	48,20	81	3705	853	0
	51,45	48,23	0	1644	1244	316
	50,49	48,91	94	2461	3426	0
	50,73	48,81	0	2331	2270	0
	50,77	48,67	0	3312	2119	206
	50,86	48,73	0	2106	2005	0
	51,14	48,51	0	2867	608	0
	50,94	48,75	226	2417	231	289
	51,45	48,28	0	2046	110	540
	50,93	48,77	0	1770	1084	163
	50,53	48,93	11	2054	3202	128
	50,30	49,37	0	1080	2222	0
	50,54	48,96	0	3133	1863	0
	50,51	49,28	102	1987	0	0
Average	50,80	48,77	73	2434	1631	118

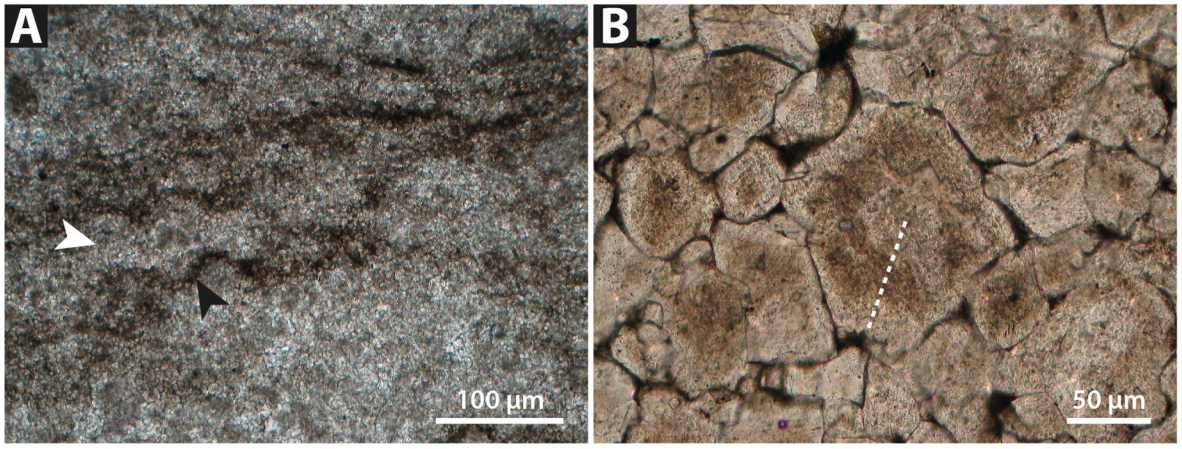

Fig. 11. A) Micritic (black arrow) to microsparitic (white arrow) dolomite of laminated bindstones (5.048 m sample), analyzed in WDS. B) Edge-core transect (white dashed line) of WDS analysis in a coarse zoned dolomite crystal showing light edges and a brownish core (xenotopic dolomite m 6067,80).

common arid climate conditions during Norian (e.g. Sellwood and Valdes, 2006). Moreover, the same model has been also proposed for the coeval deposits of the inner-shelf to transitional domains of the Dolomia Principale Fm (e.g. Frisia, 1994; Meister et al., 2013). In the sabkha-like dolomitization model, and so in the studied deposits, the pumping of sea water and/or ground water through the sediment, as well as the removing of Ca^{2+} and SO_4^{2-} ions with the precipitation of gypsum and/or anhydrite minerals, brings to an increasing the Mg/Ca ratio promoting the dolomite formation (e.g. Warren, 2000; Meister et al., 2013).

As confirmation, the stable isotopes values of the Core 1 deposits ($\delta^{13}C$ from 1.55‰ to 2.31‰ and $\delta^{18}O$ from −2‰ to −3.89‰), which overlap the isotopic range of the Norian marine carbonates (Veizer et al., 1999; Korte et al., 2005; Berra et al., 2020), further indicate that the studied deposits were dolomitized at near-surface conditions with the dolomitizing fluids significantly influenced by the contribution from the Triassic marine waters. Most probably the dolomitizing fluids were provided by the cyclical subaerial exposure of the sabkha setting, which allowed saline fluids to concentrate and circulate through the sediments. This is also testified by the high concentration of Sr (318 ppm in average) which differ from the Sr concentration of ideal dolomites precipitated from modern seawater (ca. 50–106 ppm) (Wheeler et al., 1999), but fit with the dolomites precipitated in modern similar supratidal environments of the Arabian Gulf, Bahamas and the Florida Keys (300–600 ppm) (Behrens and Land, 1972; Land and Hoops, 1973; Bein and Land, 1983). Moreover, the Na concentration of the Core 1 deposits are generally high (average of 2139 ppm) that greatly exceeds the ancient dolomites characterized by few hundreds of ppm (e.g. Tucker and Wright, 1990; Warren, 2000) and strength the interpretation of a sabkha high-saline dolomitizing fluid, characterized also by reducing

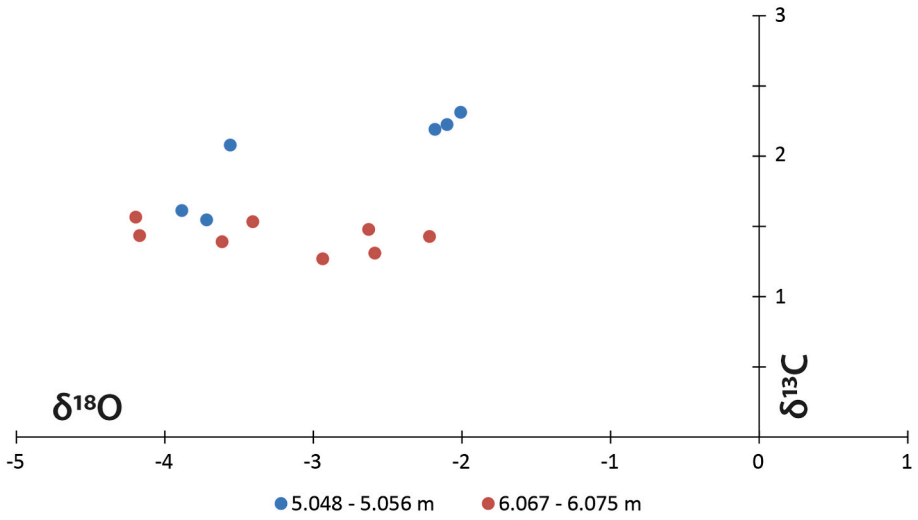

Fig. 12. Scatter diagram of $\delta^{18}O$ and $\delta^{13}C$ for the investigated dolomites coming from the shallowest (5.048–5.056 m – blue dots) and deepest (6.067–6.075 m – red dots) cores of the Puglia 1 well.

conditions, as suggested by the presence of pyrite (Fig. 7E and F) and by the high concentration of Mn (119 ppm) and Fe (211 ppm) (see also Budd, 1997).

Finally, possible localized primary micritic/microbial dolomite formation in association with the microbial mats in the sabkha setting must be also taken into account, since this process is widely documented to occur in analogous modern environments (e.g. Bontognali et al., 2010; Perri et al., 2018). Moreover, the geochemical characteristics of microbial dolomite of high-saline environments do not differ much to those observed in such studied rocks (Sánchez-Román et al., 2011; Geske et al., 2012), as well as those of other Triassic fossil primary microbial dolomites of similar environments (Mastandrea et al., 2006; Perri and Tucker, 2007).

The Core 2, unlike the Core 1, is instead characterized by the almost complete destruction of the original depositional textures and fabrics, with the presence of only ghosts of the original grains, such as shell fragments and oolites (see Chapter 5.1). However, also the isotopic composition of the Core 2 deposits ($\delta^{13}C$ from 1.27‰ to 1.57‰ and $\delta^{18}O$ from −2.22‰ to −4.2‰) falls in the isotopic range of the Norian marine carbonates (Veizer et al., 1999; Korte et al., 2005; Berra et al., 2020) - similarly to Core 1 - suggesting that they were dolomitized at near-surface conditions through the influence of concentrated Triassic marine waters (as the Na content of 2052 ppm in average and the presence of cubic to prismatic intra-crystal pores suggesting original salt inclusions - Perri et al., 2013; Slowakiewicz et al., 2016). However, the Sr concentration of 156 ppm in average, that is much lower than the average Sr concentration of the Core 1, supports the interpretation of a more marine (shoreface to offshore transition zone) depositional environment, in respect to the sabkha setting of the Core 1, in accordance with the petrographical observations. Moreover, the Core 2 deposits show Mn concentration values of 102 ppm in average and high Fe concentration (969 ppm in average). This could suggest, besides the confirmation of reducing conditions, a further external source of Fe cations from the underlying sandstones that are commonly found below the Burano Anhydrite Fm, including the Puglia 1 well (Fig. 3).

Excluding the eventual micritic primary microbial dolomite, since in both cores the dolomitization process occurred very early and at near-surface conditions, the differences in the fabric retentive and fabric destructive dolomites can be ascribed to the original depositional textures and fabrics, and consequently to the number of possible nucleation sites that drive the pseudomorphic dolomite replacement. It Is inferred that to retain the original depositional fabric lots of nucleation sites are requested to inhibit the dolomite competitive growth, whereas when nucleation sites are few, the dolomite crystals will grow extensively producing a non-pseudomorphic mosaic (e.g. SibIey, 1982; Tucker and Wright, 1990; Warren, 2000; Mastandrea et al., 2006). This can be resumed with a direct proportionality between the abundance of carbonate microcrystals (micrite) and the fabric retention potential of the dolomitization process. For this reason, the micritic microbial bindstones and the dolomudstone-dolowackestones of the Core 1 typical of sabkha setting, were favored in the preservation of the original fabric, whereas the dolopackstone/dolograinstones fabrics - poor of micrite - of the lagoonal/beach environments (e.g. shore-face to offshore transition zone) recorded in the Core 2 were almost totally destroyed.

Regarding the thermal history of the studied rocks, according to Caldarelli et al. (2013) which analyzed the Burano Anhydrite Fm in the Aquila 1 well, located few Km southeastward of the here-studied Grifone 1 well (Figs. 2 and 3), it experienced a maximum temperature spanning from 120 °C to 140 °C, reached during the late Cenozoic. The occurrence of such a similar temperature range in the studied deposits, with difference between the two cores, is testified by the almost stoichiometric composition of analyzed dolomite samples (Table 1) (e.g. Geske et al., 2012), and the development of increasing order and xenotopic textures. The change from thermodynamically less stable, non-stoichiometric, poorly-ordered dolomite, to more stable, stoichiometric, better-ordered dolomite is thought to occur during burial ("aging" - e.g. Montanez and Read, 1992; Kupecz et al., 1994; Malone et al., 1996; Al-Aasm and Packard, 2000; Warren, 2000). The Core 2 dolomites (6.067–6.075 m) that reached higher temperatures, result better ordered (and so aged) than the shallower dolomites of the Core 1 (5.048–5.056 m) (Fig. 5C and D). The temperature is also a key factor for the formation of xenotopic to idiotopic dolomite textures. In fact, at lower temperatures, the formation of smooth crystal surfaces of euhedral to subhedral crystals is energetically favored (idiotopic mosaic); whereas above the so-called "critical roughening temperature - CRT" (generally between 50 °C and 100 °C) anhedral dolomite crystal mosaic (xenotopic mosaic) generally formed (e.g. Gregg and Sibley, 1984; Sibley and Gregg, 1987; Warren, 2000). In all the studied samples of the Core 1 and Core 2, the xenotopic texture is dominant and is especially well-developed into the Core 2 which reached major temperatures than the Core 1. This confirms the burial model of Caldarelli et al. (2013) and supports the interpretation of a burial depth at least exceeding the CRT for dolomite in the Core 2.

The further mineral component of the studied deposits is anhydrite, which generally occurs in both cores as fracture and/or void filling (Figs. 7D and 8G, H), and as lenticular and/or tabular crystals forming

mm-thick levels within the laminated microbial bindstones of the Core 1 (Fig. 6E and F). The diagenesis of sulphates is commonly very articulated since the transformation from gypsum to anhydrite and *vice versa* (i.e. dehydration-hydration process) can occur multiple times depending on the burial and uplift conditions (e.g. Testa and Lugli, 2000). Temperature exceeding 51 °C, generally reached in the shallow burial, is sufficient for the gypsum–anhydrite conversion (e.g. Hardie, 1967; Testa and Lugli, 2000) and in these conversions, very common relicts (inclusions) of the original mineral can survive into the new crystal cores. In the studied rocks, the only examples of these kind of relicts occur in the anhydrite crystal levels of the microbial bindstones of the Core 1 (Fig. 6F), whereas the fracture/void filling anhydrite, in both cores, is generally characterized by a clear habit without any signs of inclusions (Fig. 6B; 8C; 10 E, F). This suggests that the anhydrite crystals levels of Core 1 were subjected to a hydration-dehydration process, whereas the fracture/void filling anhydrite is a primary precipitated during shallow

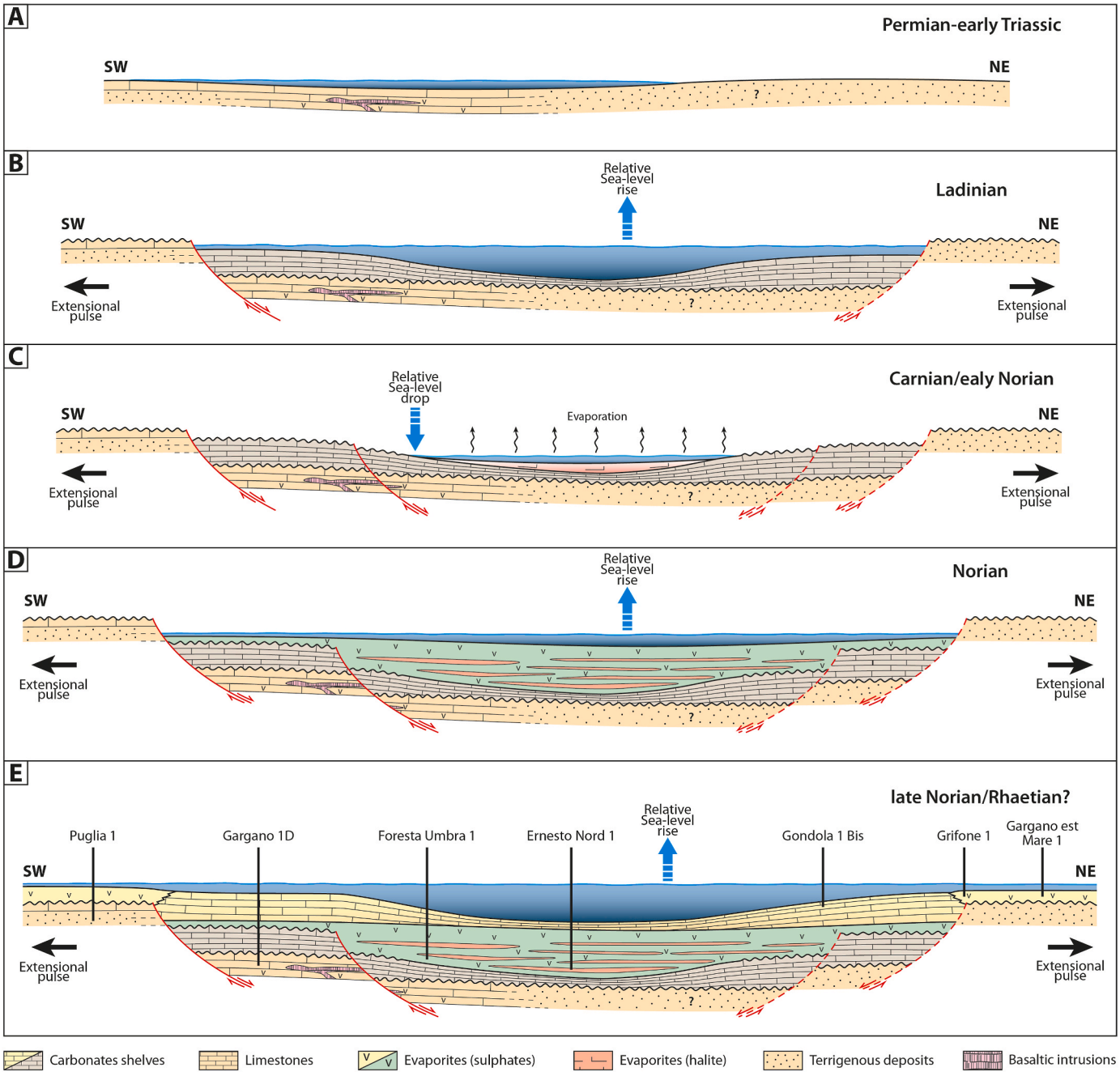

Fig. 13. Idealized Permian to Rhaetian stratigraphic and depositional model of the Southern Adriatic sector. A) During Permian widespread continental conditions persisted in the study area. In the late Permian-early Triassic a marine ingression brought to the development of coastal lagoons characterized by carbonate deposition. B) In the Ladinian, after a generalized erosional phase, an extensional tectonic pulse of the neo-forming western Tethys branch, led to a relative sea-level rise that triggered the formation of a carbonate shelf in the resultant tectonic depression. C) During Carnian-early Norian a further extensional tectonic pulse and a relative sea-level drop brought to the isolation of a basin, erosion above the old shelf margins (mid-Triassic unconformity) and to the establishment of enhanced salinity and evaporative conditions, which in turn led to the deposition of evaporites (halite and sulphates). D) The progression of the extension and the relative sea-level rise of the Norian induced a progressive filling of the newly formed depocenter by shallow-water evaporites (e.g. Basin Fill Evaporites). E) In the late Norian-Rhaetian a general sea-level rise restored the connections with the open-sea and shifted the evaporite deposition to the margins of the basins that previously remained under subaerial conditions. Along these margins wide sabkha settings, making sea-ward transition to carbonate platforms, developed.

to deep burial, after the reaching the temperature limit of 51 °C. According to the burial history of Caldarelli et al. (2013), a similar temperature was already reached during the early Jurassic, and since then all the voids and fractures were filled by anhydrite.

Moreover, as the presence of a sulphate-rich diagenetic fluid, the precipitation of burial dolomite that commonly occur in other coeval Norian Western Tethys deposits (e.g. Berra et al., 2020) was inhibited.

The fracturing could have occurred in any moment of the early burial history because of tectonics and/or isostatic adjustments that could have brought to the formation of decompression fractures filled by anhydrite, and also new compression which was responsible for the pressure-solution process and the formation of stylolites (Fig. 6B and C; 8D).

On the contrary, the presence of relicts in the anhydrite crystals of the microbial bindstones (Fig. 6F) suggests a more articulated diagenetic history: In fact, if the primary depositional mineralogy of these crystals could be matter of speculation, they were at least characterized by one cycle of hydration-dehydration. Considering that the relicts within the anhydrite crystals are composed of anhydrite as the crystal that contains them, this implies that the firsts sulphate crystals precipitated as anhydrite (primary) in the sabkha setting (see chapter 5.1), and then anhydrite was transformed into gypsum, because of meteoric water percolating into the sediments and the fluctuation of the groundwater brine concentration, with relicts of the original anhydrite crystal in the center of the newly formed gypsum. Successively, during burial, the

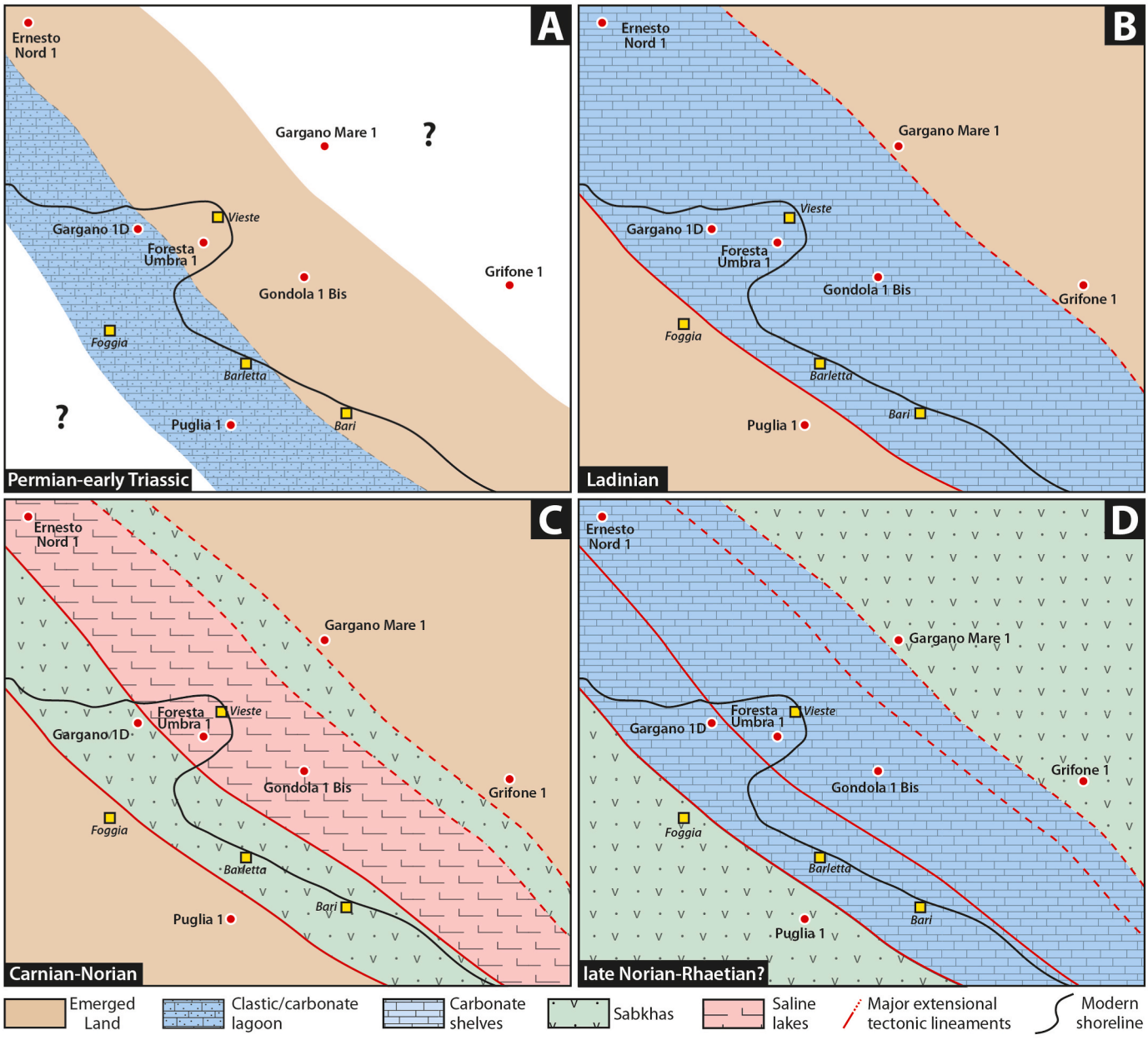

Fig. 14. Inferred paleogeographic evolution of the Southern Adriatic sector from late Permian up to Rhaetian. A) During late Permian-early Triassic a marine ingression in the continent brought to the development of coastal lagoons. B) In the Ladinian, after a generalized erosional phase, an extensional tectonic pulse brought to the formation of NW-SE oriented extensional faults and to a resultant tectonic depression in which a carbonate shelf developed. C) During Carnian-Norian a further extensional tectonic pulse and a relative sea-level drop brought to the isolation of the basin and to the establishment of enhanced salinity and evaporative conditions. In the newly formed depocenter zone a saline lake formed, making transition both southwestward and northeastward to sabkha settings. D) In the late Norian-Rhaetian a general sea-level rise, restored the connections with the open-sea and shifted the evaporite deposition towards the parts of the basin that previously were under subaerial conditions. These latter were characterized by wide sabkha settings, making sea-ward transition to carbonate platforms.

gypsum is dehydrated and re-transformed into anhydrite (secondary) which consequently hosts internal inclusions of primary (depositional) anhydrite.

5.3. Facies distribution and paleogeographic evolutionary model

On the base of the presented dataset, an attempt of construction of an integrated sedimentary-stratigraphic (Fig. 13) and paleogeographic (Fig. 14) model of the Southern Adriatic sector, spanning from late Permian to late Triassic, is here discussed. Unfortunately, the available dataset on the Permian-Triassic of Southern Adriatic is very poor, such as the existing bibliography with only few works based on large scale subsurface dataset such as wells and seismics (e.g. Martinis and Pieri, 1964; Ciarapica et al., 1987; De Dominicis and Mazzoldi, 1989; Finetti and Del Ben, 2005; Scisciani and Calamita, 2009; Santantonio et al., 2013; Festa et al., 2014; Teofilo et al., 2016; Morsilli et al., 2017). For these reasons, the presented model (Figs. 13 and 14) could result highly speculative and possibly subject to future changes.

The investigated area covers a transect of 250 km from SE to NW and 150 Km from NE to SW and is representative of the innermost part of the Adria microplate (Vai, 2001; Golonka, 2004; Finetti, 2005) which can be compared with other coeval terranes of the Western Tethys such as the Alpine realm (e.g. Bosellini et al., 2003; Russo et al., 2006; Stefani et al., 2010), the Calabria setting (e.g. Ietto et al., 1995; Iannace et al., 1995, 2005; Mastandrea et al., 2003; Perri et al., 2017, 2019; Borrelli et al., 2019, 2023) or the Croatian, Albanian and Greek areas (e.g. Cota and Baric, 1998; Grandić et al., 2002, 2013; Velić et al., 2015; Vlahović et al., 2005; Wrigley et al., 2015; Scisciani and Esestime, 2017; Koch, 2020; Kamberis et al., 2022).

During Permian, the global paleogeography was extensively influenced by late Paleozoic collision (mid Carboniferous – early Permian) of Laurasia with the north Gondwana that brought to the formation of the Central Pangean Mountain belt (e.g. von Raumer et al., 2012; Stampfli et al., 2013; Scotese and Schettino, 2017). This latter was oriented nearly parallel to the Equator and at its south-eastern foothills, where most of the central-western Mediterranean terranes were inferred to be located (comprised the Adria microplate), the northern shore of the neo-forming western Tethys developed (e.g. Ziegler et al., 1997; Dercourt et al., 2000; Scotese and Schettino, 2017).

In the studied dataset, only two wells penetrated up to the Permian deposits (Puglia 1 and Gargano 1) revealing a mainly transition from terrigenous to carbonate sediments (Fig. 3) and so a transgressive evolution of the sedimentary system. The terrigenous deposits, sometimes characterized by red beds, testify a continental environment (e.g. alluvial fans, flood plains) with an enhanced clastic input deriving from the dismantling of the Central Pangean Mountain belt (Figs. 13A and 14A). On the contrary, the carbonate deposits generally indicate shallow-water to coastal lagoon environments (Figs. 13A and 14A). This transgressive evolution can be ascribed to the Permian oceanic spreading of the Tethys realm, whose activity is also testified by the presence of basaltic intrusions in the Permian sedimentary succession. In fact, despite a global sea-level lowering (Haq et al., 1988), the break-up of the Pangea due to the western Tethys rift, brought to a generalized subsidence and to the westward oriented marine ingression through the continent (Scisciani and Esestime, 2017), that progressively changed the sedimentary environments of deposition from mainly clastic to evaporitic and carbonate. As a consequence, the Alpine realm, located north-westward in respect to the Adria microplate, was characterized at the end of the Permian/early Triassic by entirely clastic deposits in the central Alps (Verrucano Lombardo and Val Gardena Sandstone) (e.g. Cassinis and Neri, 1992; Virgili et al., 2006; Cassinis and Perotti, 2007; Gretter et al., 2013) and mainly carbonate and evaporites in the eastern Alps and Dolomites (Bellerophon Fm.) (e.g. Bosellini et al., 2003; Stefani et al., 2010; Ronchi et al., 2018). The Adria microplate (Southern Adriatic) resulted more affected by the Tethyan marine ingression that brought to a progressive shifting from a diffuse continental clastic sedimentation to shallow-water and lagoonal carbonate deposition (Figs. 13A and 14A). In fact, the clastic-carbonate dominated deposition persisted up to the Early Triassic, as recorded by the reddish conglomerate, arenites and silty-claystones attributed to the Werfen Fm (Eni nomenclature) in the Puglia 1 well (Fig. 3). The Werfen Fm, for stratigraphic position and lithological analogies can be compared with the Early Triassic Werfen Fm of the Dolomites (Stefani et al., 2010; Ronchi et al., 2018), suggesting that in the Early Triassic, the progression of the marine ingression of the western Tethys reached also the Alpine realm.

After the Early Triassic, a generalized erosional phase involved the study area, as testified by the stratigraphic hiatus occurring up to the Ladinian in the Gargano 1D well and up to the Late Triassic in the Puglia 1 well (Fig. 3). This difference in the restart of sedimentation, can be ascribed to a differential subsidence triggered by the formation of NW-SE trending extensional faults, as also testified by the CROP M13 line (Fig. 4), of the western Tethys rifting (e.g. Ciarapica and Passeri, 2002; Fantoni and Franciosi, 2010) (Figs. 13B and 14B). In fact, during the Ladinian, an extensional tectonic pulse coupled with a global sea-level rise (Haq et al., 1988), led to the formation of a tectonic depression (extensional intra-platform basin) bordered by two tectonic highs, probably represented by the Apulia Platform to the W and by the Adriatic Platform to the E (see Tari, 2002), and also to the consequent marine ingression (relative sea-level rise). This latter, as testified by the Gargano 1D carbonate deposits, brought to the development of a complete carbonate shelf probably characterized by inner platform to basin setting (Figs. 13B and 14B), as also suggested by the thickness differences of the mid Triassic succession in the CROP M13 line (Fig. 4). In any case, southwestward of the depression, as suggested by the absence of Ladinian deposits in the Puglia 1 well (Fig. 3), and probably also northeastward, subaerial conditions still persisted and no sedimentation occurred (Figs. 13B and 14B).

During the Ladinian extensive carbonate platform systems developed in the neo-forming western Tethys realm, indicating a generalized transgression phase. This is testified by the Sciliar and Livinallongo Fms of the Alpine realm (e.g. Bosellini et al., 2003; Stefani et al., 2010; Abbas et al., 2018) and also by the San Donato Unit Ladinian reef-complex of the Calabrian terranes (e.g. Boni et al., 1990; Iannace et al., 1995, 2005).

Successively, during the Carnian-Norian, widespread evaporitic conditions settled in the study area, as testified by the anhydrite dominated deposits of the Gargano 1D, Foresta Umbra 1 and Ernesto Nord 1 wells (Fig. 3). In particular, the Foresta Umbra 1 and Ernesto Nord 1 wells, show an enhanced thickness of the anhydrite dominated body in respect to the Gargano 1D well, suggesting the presence of a depocenter in their correspondence (Figs. 13C and 14C). This latter, most probably originated as consequence of another extensional pulse of the western Tethys rift which created a further NW-SE oriented extensional faults system in the southwestern part of the studied setting and probably also in its northeastern zone (Figs. 13C and 14C). These fault systems are also highlighted in the CROP M13 line (Fig. 4) where multiple NW-SE trending normal faults developed during Triassic influencing the sedimentary filling of the basin (e.g. Finetti and Del Ben, 2005; Scisciani and Calamita, 2009; Santantonio et al., 2013). Moreover, as consequence of the Carnian-Norian relative sea-level drop, the connections with the open sea were interrupted, a marked erosional surface formed (mid Triassic unconformity in the CROP M13 line – Fig. 4) and new isolated basin developed (Figs. 13C and 14C). This renewed basin-physiography, coupled with climate arid conditions which in turn enhanced evaporation, brought to the development of widespread sabkha settings and hypersaline lakes (Fig. 13C). This is testified by the common presence of halite and anhydrite in the Ernesto Nord 1 and Foresta Umbra 1 wells (Fig. 3). During the Norian the progression of the extension brought to a relative sea-level rise which gradually contributed to the filling of the depocenter (e.g. Basin Fill Evaporites *sensu* Gindre-Chanu et al., 2020; Borrelli et al., 2022) through the deposition of generally shallow-water evaporites (both halite and anhydrite) that through times also reached the margins, less affected by the tectonic subsidence and consequently

not part of the main depozone (Fig. 13D). This is the reason why the Foresta Umbra 1 and Ernesto Nord 1 (depocenter) show an enhanced thickness of the anhydrite dominated body in respect to the Gargano 1D (margin) (Fig. 3). At this time, the south-westernmost part of the study area (Apulia Platform) was, most probably, still under subaerial conditions with no deposition of sediments, possibly as the corresponding north-easternmost zone (Adriatic Platform) (Fig. 14D).

The environmental and sedimentary conditions of the studied area during Carnian-Norian completely differs from the Calabrian and Alpine contexts. In the Calabrian terranes, during the Carnian, evaporitic conditions, similar to the one proposed for the Southern Adriatic setting developed, with the formation of an evaporitic-carbonate platform (Scifarello Unit) (Iannace et al., 1995, 2005; Perri et al., 2019). However, during Norian the evaporite deposition was already interrupted and microbial dominated carbonate shelves developed (Corvino and Vaccuta Unit) (Perri et al., 2019), suggesting a major effect of the tectonic subsidence in this area in comparison with the South Adriatic. Instead in the Alpine realms, during the Carnian-Norian the peritidal carbonates of the Dolomia Principale Fm developed, essentially with limited evaporitic deposition testified by the San Giovanni Bianco Fm and some facies of Raibl (e.g. Bosellini and Hardie, 1973; Berra and Jadoul, 2002; Berra and Siletto, 2006), and continued until the Rhaetian (e.g. Bosellini et al., 2003; Stefani et al., 2010; Abbas et al., 2018).

Lastly, in the late Norian-Rhaetian, carbonate deposition re-established as highlighted by the Gargano 1D, Foresta Umbra 1, Ernesto Nord 1 and Gondola 1 Bis wells, whereas the evaporitic deposition shifted in the south-westernmost (Puglia 1 well) and in the north-easternmost (Grifone 1 and Gargano Est Mare 1) sectors (Fig. 3). This changing in the depositional style could be potentially due to a relative sea-level rise triggered by a more effective extensional tectonic subsidence and overcoming the Norian-Raethian global sea-level drop (Haq et al., 1988). As a consequence, the marine connections with the sea were re-established and new carbonate platforms developed, whereas the evaporite deposition was shifted and limited in the marginal parts of the basin (Figs. 13E and 14D). In particular, the thicker carbonate succession of the Gargano 1D, also showing the presence of macrofossils such as corals, could suggest the presence of an inner to margin setting of a carbonate shelf, whereas the thinner carbonate succession of Foresta Umbra 1 and Ernesto Nord 1 with argillaceous to shaly levels possibly account a slope context (Figs. 3 and 13E). On the contrary, the coeval anhydrite dominated deposits of the Puglia 1 well, also according to the facies analysis (see Chapter 5.1) are indicative of a sabkha setting, which settles directly above the Lower Triassic deposits (Fig. 3) because the sea-level reached this part of the basin only in the late Norian-Rhaetian (Figs. 13E and 14D). The same configuration of Puglia 1 is inferred also for the north-easternmost Grifone 1 and Gargano Est Mare 1 wells, which also show in their uppermost part anhydrite dominated deposits (Fig. 3), suggesting a similar sedimentary history of the Puglia 1 well.

The Norian-Rhaetian relative sea-level rise is effectively recorded also in the Calabrian terranes and in the Alpine realm, both showing the presence of a carbonate dominated deposition without the presence of evaporites. In particular, during late Norian in the Calabrian area, carbonate ramps with a dominant retrograding architecture developed (Perri et al., 2019). They testify a relative sea-level rise that culminated successively, in the Rhaetian, with the drawing of the carbonate platforms and the turnover towards mainly deep-water environments of deposition (Perri et al., 2019). A similar evolution also happened in the Alpine realm, which since Carnian up to Norian was characterized by the monotonous deposition of the peritidal carbonates of the Dolomia Principale Fm (e.g. Bosellini et al., 2003; Stefani et al., 2010). However, during Rhaetian a relative sea-level rise brought firstly to the development of the Dachstein limestone carbonate platform which were lately overlain by the basinal deposits of the Calcari Grigi and Ammonitico Rosso Fms (e.g. Bosellini et al., 2003; Gianolla et al., 2008). Consequently, despite all the reported settings (Southern Adriatic, Calabrian terrane and Alpine realm) record a relative sea-level rise, the southern Adriatic resulted less affected by this late Triassic sea-level change and consequently developed different depositional environments, in respect to the Calabrian and Alpine realm which generally reached deep-water environmental conditions.

According to the proposed sedimentary and paleogeographic model, great attention must be paid to the correlation of the Triassic sedimentary bodies since lateral variations in the sedimentary succession both regarding the thickness and the lithologies could be very important (Fig. 13). In fact, the uppermost Late Triassic dolomite dominated body (dolomitic member according to ENI nomenclature) characterized by more than 2.300 m of thickness in the Gargano 1D wells and by ca. 600–800 m of thickness in the Foresta Umbra 1 and Ernesto Nord 1 well, results coeval with the anhydrite dominated succession in the Puglia 1 well (Fig. 3). This latter, despite it is lithologically similar to the main anhydrite dominated body found in the Gargano 1D, Foresta Umbra 1 and Ernesto Nord 1 well (Fig. 3), is temporally subsequent, and consequently not stratigraphically correlatable. This implies and suggests that for the regional stratigraphic correlations it is fundamental to consider the complete 3D architecture of the sedimentary bodies, since they are commonly characterized by internal lithological variations which can potentially create misunderstandings in the correlations.

6. Conclusion

The Southern Adriatic province represents the innermost part of the Adria microplate and also a key area for the E&P companies that, since the 70's, drilled several well boreholes. Seven of these wells, which penetrated up to more than 6 Km, were studied in order to uncover the sedimentary and paleogeographic evolution of this part of the Adria microplate during the end of Permian-Triassic interval, with direct implications on the extension of potential hydrocarbon reservoirs in the area.

Widespread continental conditions, intermittently changing towards the development of coastal lagoons characterized by carbonate deposition, occurred during the final stage of the Permian. Then, in the Ladinian, after a generalized erosional phase, an extensional tectonic pulse of the neo-forming western Tethys branch, led to a relative sea-level rise and to the formation of a carbonate shelf in the resultant NW-SE oriented tectonic depression. During Carnian-early Norian a further extensional tectonic pulse, accompanied by a relative sea-level drop, brought to the isolation of the basin and to the establishment of enhanced salinity and evaporative conditions which in turn led to the deposition of evaporite deposits (halite and sulphates). The progression of the extension and the successive relative sea-level rise of the Norian led to a progressive filling of the newly formed depocenter by evaporites (i.e. Basin Fill Evaporites). Lastly, In the late Norian-Rhaetian, a general sea-level rise restored the connections with the open-sea and shifted the evaporite deposition to the margins of the basins, that previously remained under subaerial conditions.

Among all the studied wells, it was possible to sample two cores, both recovered from the Puglia 1 borehole, that permitted to characterize the sedimentological facies and diagenetic processes that affected some intervals of the Burano Anhydrite Fm. The first, shows the presence of lenticular/tabular shaped anhydrite crystals immersed within a dolomudstone with remnants of thinly laminated microbial laminas, suggesting a sabkha-type environment of formation. On the contrary, the second, is generally characterized by massive coarse-grained crystalline dolomite with some remnants of oolites and undetermined shell fragments, indicating a marine shallow-water environment of deposition (e.g. shore-face/offshore transition setting).

Syn-sedimentary and late-stage diagenetic processes affected these deposits: primary anhydrite crystals deposited in the sabkha setting very early but, were lately affected at least by one hydration-dehydration cycle during the burial phase; whereas, fracture-filling anhydrite is a later-stage diagenetic product of circulating sulphate-rich fluids. Dolomitization is pervasive in the studied cores and, as suggested by the

isotope values of $\delta^{13}C$ and $\delta^{18}O$ which overlap the isotopic range of the Norian marine carbonates, most probably occurred very early under near-surface conditions as the circulation of high saline dolomitizing fluids under general reducing conditions. This dolomitization resulted influenced by the original carbonate sedimentary textures since original micrite was replaced by fabric-preserving dolomite and, coarser sediments by fabric-destructive microspar to spar dolomite. The early-dolomitization preserved the studied deposits by major burial diagenetic transformation permitting only the development of xenotopic texture and ordered dolomite crystals together with limited aggrading neomorphism.

Authors contribution statement

MB and EP are the main authors of work, realizing all research parts and the manuscript. SC helped in the sampling and in writing the text. MM helped in the revision and writing of the text.

Declaration of competing interest

The authors declare that they have no known competing financial interests or personal relationships that could have appeared to influence the work reported in this paper.

Data availability

Data will be made available on request.

Acknowledgements

We gratefully acknowledge the critical and constructive comments of the Editor in Chief Massimo Zecchin and two anonymous reviewers that greatly helped in the improvement of the final version of the manuscript. We also thank ENI S. p.A. for the access to the data presented in the paper. We acknowledge Giovanna Scopelliti from the University of Palermo DiSTeM (Dipartimento di Scienze della Terra e del Mare) for the isotopic analysis and Mariano Davoli from the Università della Calabria DiBEST (Dipartimento di Biologia, Ecologia e Scienze della Terra) for the SEM and WDS analysis. Financial support for this research derived from MIUR (ex 60%) funds (resp. E. Perri and S. Critelli) and from PON React-EU "Ricerca e Innovazione" 2014–2020 funds (CUP: H25F21001220006).

References

Abbas, H., Michail, M., Cifelli, F., Mattei, M., Gianolla, P., Lustrino, M., Carminati, E., 2018. Emplacement modes of the Ladinian plutonic rocks of the Dolomites: insights from anisotropy of magnetic susceptibility. J. Struct. Geol. 113, 42–61.

Al-Aasm, I., Packard, J.J., 2000. Stabilization of early-formed dolomite: a tale of divergence from two Mississippian dolomites. Sediment. Geol. 131, 97–108.

Al-Aasm, I., Taylor, B.E., South, B., 1990. Stable isotope analysis of multiple carbonate samples using selective acid extraction. Chem. Geol. 80, 119–125.

Al-Belushi, J., Glennie, K.W., Williams, B.P.J., 2016. Permo-Carboniferous glaciogenic Al Khlata Formation, Oman: a new Hypothesis for origin of its glaciation. GeoArabia 1, 389–403.

Anelli, L., Mattavelli, L., Pieri, M., 1996. Structural–stratigraphic evolution of Italy and its petroleum systems. In: Ziegler, P.A., Horvath, F. (Eds.), Peri-Tethys Memoir 2, vol. 170. Mem. Mus. Natur. Hist. Mat., pp. 455–483

Angiolini, L., Balni, M., Garzanti, E., Nicora, A., Tintori, A., 2003. Gondwanan deglaciation and opening of Neotethys: palaeontological and sedimentological evidence from interior Oman. Palaeogeogr. Palaeoclimatol. Palaeoecol. 196, 99–123.

Angiolini, L., Gaetani, M., Muttoni, G., Stephenson, M.H., Zanchi, A., 2007. Tethyan oceanic currents and climate gradients 300 m.y. ago. Geology 35, 1071–1074.

Aref, M., Taj, R., 2018. Recent evaporite deposition associated with microbial mats, Al-Kharrar supratidal–intertidal sabkha, Rabigh area, Red Sea coastal plain of Saudi Arabia. Facies 64, 28.

Battaglia, M., Murray, M.H., Serpelloni, E., Burgmann, R., 2004. The Adriatic region: an independent microplate within the Africae-Eurasia collision zone. Geophys. Res. Lett. 31.

Behrens, E.W., Land, L.S., 1972. Subtidal holocene dolomite baffin Bay, Texas. J. Sediment. Petrol. 42, 155–161.

Bein, A., Land, L.L., 1983. Carbonate sedimentation and diagenesis associated with Mg–Ca–chloride brines: the permian san andreas formation in the Texas panhandle. J. Sediment. Petrol. 53, 243–260.

Berra, F., Azmy, K., Della Porta, G., 2020. Stable-isotope and fluid inclusion constraints on the timing of diagenetic events in the dolomitized Dolomia Principale inner platform (Norian, Southern Alps of Italy). Mar. Petrol. Geol. 121, 104615.

Berra, F., Jadoul, F., 2002. Sedimentological and paleontological evidences of a Mid Carnian transgression in the Western Southern Alps (S. Giovanni B. Fm. Lombardy, Italy): stratigraphic and paleogeographic implications. Riv. Ital. Paleontol. Stratigr. 108, 119–131.

Berra, F., Jadoul, F., Anelli, A., 2010. Environmental control on the end of the Dolomia Principale/Hauptdolomit depositional system in the central Alps: coupling sea-level and climate changes. Palaeogeogr. Palaeoclimatol. Palaeoecol. 290, 138–150.

Berra, F., Siletto, G.B., 2006. Controllo litologico e stratigrafico sull'assetto strutturale delle Alpi meridionali lombarde: il ruolo degli orizzonti di scollamento. Rendicont. Soc. Geol. Ital. 2, 78–80.

Bertello, F., Fantoni, R., Franciosi, R., Gatti, V., Ghielmi, M., Pugliese, A., 2010. From thrust-and-fold belt to foreland: hydrocarbon occurrences in Italy. Petrol. Geol. Conf. series 7, 113–126.

Bertotti, G., Picotti, V., Bernoulli, D., Castellarin, A., 1993. From rifting to drifting: tectonic evolution of the south-Alpine upper crust from the Triassic to the Early Cretaceous. Sediment. Geol. 86, 53–76.

Boni, M., Torre, M., Zamparelli, V., 1990. Il trias medio superiore dell'Unità di San Donato (appennino meridionale, Calabria): risultati preliminari. Rendicont. Soc. Geol. Ital. 13, 89–92.

Bontognali, T.R.R., Vasconcelos, C., Warthmann, R.J., Bernasconi, S.M., Dupraz, C., Strohmenger, C.J., McKenzie, J.A., 2010. Dolomite formation within microbial mats in the coastal sabkha of Abu Dhabi (United Arab Emirates). Sedimentology 57, 824–844.

Borrelli, M., Campilongo, G., Critelli, S., Perrotta, D.I., Perri, E., 2019. 3D nanopores modeling using TEM-tomography (dolostones – upper Triassic). Mar. Petrol. Geol. 99, 443–452.

Borrelli, M., Manzo, E., Santagati, S., Perri, E., 2023. Biosedimentary and palaeoecological characterization of norian bioconstructions (western Tethys, north Calabria). Rendiconti online della Società Geologica Italiana 59. https://doi.org/10.3301/ROL.2023.08.

Borrelli, M., Perri, E., Avagliano, D., Coraggio, F., Critelli, S., 2022. Paleogeographic and sedimentary evolution of north calabrian basins during the messinian salinity crisis (South Italy). Mar. Petrol. Geol. 141, 105726.

Borrelli, M., Perri, E., Critelli, S., Gindre-Chanu, L., 2021. The onset of the Messinian Salinity Crisis in the central Mediterranean recorded by pre-salt carbonate/evaporite deposition. Sedimentology 68, 1159–1197.

Boschetti, T., Cortecci, G., Toscani, L., Lacumin, P., 2011. Sulfur and oxygen isotope compositions of Upper Triassic sulfates from northern Apennines (Italy): paleogeographic and hydrogeochemical implications. Geol. Acta 9, 129–147.

Bosellini, A., Gianolla, P., Stefani, M., 2003. Geology of the dolomites. Episodes 26, 181–185.

Bosellini, A., Hardie, L.A.W., 1973. Depositional theme of a marginal marine evaporite. Sedimentology 20, 5–27.

Bosellini, A., Morsilli, M., Neri, C., 1999. Long-term event stratigraphy of the Apulia platform margin (upper jurassic to eocene, Gargano, southern Italy). J. Sediment. Res. 69, 1241–1252.

Budd, D.A., 1997. Cenozoic dolomites of carbonate islands: their attributes and origin. Earth Sci. Rev. 42, 1–47.

Caldarelli, C., Martini, P., Smith, D., 2013. Source Rock Potential and Maturity Modelling in the Southern Adriatic Sea Area: Key Controls for Predicting Hydrocarbon Distribution. AAPG European Regional Conference & Exhibition, Barcelona, Spain.

Campana, F., Fantoni, R., Masetti, D., Scotti, P., 2017. Stratigraphic and naphthogenic characterization of the Sparviero 1 bis Mesozoic succession (southern Adriatic basin, Italy). J. Mediterr. Earth Sci. 9, 89–93.

Carminati, E., Corda, L., Mariotti, M., Scifoni, A., Trippetta, F., 2013. Mesozoic syn- and post-rifting evolution of the Central Apennines, Italy: the role of Triassic evaporites. J. Geol. 121, 327–354.

Caruso, A., Pierre, C., Blanc-Valleron, M.M., Rouchy, J.M., 2015. Carbonate deposition and diagenesis in evaporitic environments: the evaporative and sulphur bearing limestones during the settlement of the Messinian salinity crisis in Sicily and Calabria. Palaeogeogr. Palaeoclimatol. Palaeoecol. 429, 136–162.

Caruso, A., Pierre, C., Blanc-Valleron, M.M., Rouchy, J.M., 2016. Reply to the comment on "Carbonate deposition and diagenesis in evaporitic environments: the evaporative and sulphur-bearing limestones during the settlement of the Messinian Salinity Crisis in Sicily and Calabria" by Caruso et al. Palaeogeogr. Palaeoclimatol. Palaeoecol. 459, 597–605.

Casero, P., 2004. Structural setting of petroleum exploration plays in Italy. Ital. Geol. Soc. Spec 189–199.

Casero, P., Bigi, S., 2013. Structural settings of the Adriatic basin and the main related petroleum exploration plays. Mar. Petrol. Geol. 42, 135–147.

Cassinis, G., Neri, C., 1992. Sedimentary and palaeotectonic evolution of some Permian continental basins in the central Southern Alps. Italy. Cuad Geol Iber 16, 145–176.

Cassinis, G., Perotti, C.R., 2007. A stratigraphic and tectonic review of the Italian Southern Alpine Permian. Palaeoworld 16, 140–172.

Cavazza, W., Roure, F., Ziegler, P.A., 2004. The Mediterranean area and the surrounding regions: active processes, remnants of former Tethyan oceans and related thrust belts. In: Cavazza, W., Roure, F., Spakman, W., Stampfli, G.M., Ziegler, P.A. (Eds.), The TRANSMED Atlas: the Mediterranean Region from Crust to Mantle. Springer, pp. 1–29.

Cazzini, F., Dal Zotto, O., Fantoni, R., Ghielmi, M., Ronchi, P., Scotti, P., 2015. Oil and gas in the adriatic foreland, Italy. J. Petrol. Geol. 38 (3), 255–279.
Centamore, E., Deiana, G., Micarelli, A., Potetti, M., 1986. Il trias-paleogene delle marche. Studi Geol. Camerti 9–27.
Channell, J.E.T., Muttoni, G., Kent, D.V., 2022. Adria in mediterranean paleogeography, the origin of the ionian sea, and permo-triassic configurations of Pangea. Earth Sci. Rev. 230, 104045.
Ciarapica, G., Cirilli, S., Passeri, L., Trincianti, E., Zaninetti, L., 1987. Anidriti di Burano et Formation du Monte Cetona (nouvelle formation), biostratigraphie de deux series-types du Trias superieur dans l'Apennin septentrional. Rev. Paleobiol. 6, 341–409.
Ciarapica, G., Passeri, L., 2002. The paleogeographic duplicity of the Apennines. Bollettino della Societa Geologica Italiana 121 (1), 67–75.
Clifton, H.E., 2006. A reexamination of facies models for clastic shorelines. In: Posamentier, H.W., Walker, R.G. (Eds.), Facies Models Revisited, vol. 84. SEPM Special Publication, pp. 293–337.
Cota, L., Baric, G., 1998. Petroleum potential of the Adriatic offshore, Croatia. Org. Geochem. 29, 559–570.
Cruz, F.E., Eberli, G.P., 2019. Co-existence of skeletal and ooid shoals as a result of antecedent topography—cat Cay shoal complex, Bahamas. Deposit. Record 5, 451–468.
De Dominicis, A., Mazzoldi, G., 1989. Interpretazione geologico-strutturale del margine orientale della Piattaforma Apula. Mem.Soc. Geol. Ital. 38, 163–176.
Delfrati, L., Falorni, P., Groppelli, G., Petti, F.M., 2002. Carta Geologica d'Italia 1:50.000. Catalogo delle formazioni. Fascicolo III - unità validate. Quaderni del Servizio Geologico d'Italia, Serie III 7 (3), 208.
Dercourt, J., Gaetani, M., Vrielynck, B., Barrier, E., Biju-Duval, B., Brunet, M.-F., Cadet, J.P., Crasquin, S., Sandulescu, M., 2000. Atlas Peri-Tethys Paleoegeographical Maps. CCGM/CGMW, Paris, pp. 1–269.
Doglioni, C., Carminati, E., Cuffaro, M., 2006. Simple kinematics of subduction zones. Int. Geol. Rev. 48 (6), 479–493.
El-Tabakh, M., Ricconi, R., Schreiber, B.C., 1997. Evolution of late triassic basin evaporites (passaic formation) newark basin, eastern north America. Sedimentology 44, 767–790.
El-Tabakh, M., Schreiber, B.C., Warren, J.K., 1998. Origin of fibrous gypsum in the Newark rift basin, eastern North America. J. Sediment. Res. 68, 88–99.
Faccenna, C., Jolivet, L., Piromallo, C., Morelli, A., 2003. Subduction and the depth of convection in the Mediterranean mantle. J. Geophys. Res. 108 (B2).
Fantoni, R., Franciosi, R., 2010. Tectono-sedimentary setting of the Po plain and adriatic foreland. Rend. Fis. Accad. Lincei 21 (1), 197–209.
Fantoni, R., Bersezio, R., Forcella, F., 2004. Alpine structure and deformation chronology at the southern Alps – Po plain border in Lombardy. Bollettino Società Geologica Italiana 123, 463–476.
Fantoni, R., Catellani, D., Merlini, S., Rogledi, S., Venturini, S., 2002. La registrazione degli eventi deformativi cenozoici nell'avampaese veneto-friulano. Mem. Soc. Geol. It. LVII, 301–313.
Festa, V., Teofilo, G., Tropeano, M., Sabato, L., Spalluto, L., 2014. New insights on diapirism in the Adriatic Sea: the Tremiti salt structure (Apulia offshore, southeastern Italy). Terra. Nova 26, 169–178.
Finetti, I., 1982. Structure, stratigraphy and evolution of central mediterranean. Boll. Geof. Teor. Appl. 24, 247–426.
Finetti, I., 2005. CROP Project: deep seismic exploration of the central mediterranean and Italy. Atlases Geosci. 1, 1–794.
Finetti, I.R., Del Ben, A., 2005. Crustal Tectono-Stratigraphic setting of the Adriatic Sea from new CROP seismic data. In: Finetti, I.R. (Ed.), CROP Project: Deep Seismic Exploration of the Central Mediterranean and Italy. Atlases in Geoscience 1. Elsevier, New York, pp. 519–548.
Frisia, S., 1994. Mechanisms of complete dolomitization in a carbonate shelf: comparison between the norian Dolomia Principale (Italy) and the holocene of abu dhabi sabkha. In: Purser, B., Tucker, M.E., Zenger, D. (Eds.), A Volume in Honour of Dolomieu, vol. 21. Int. Assoc. Sedimentol. Spec. Publ., pp. 55–74
Garzanti, E., 1999. Stratigraphy and sedimentary hystory of Nepal Tethys Himalayan passive margin. In: Upreti, B.N., Le Fort, P. (Eds.), Advances on the Geology of the Himalaya – Focus on Nepal, vol. 17. Journal of Asian Earth Sciences, pp. 805–827.
Garzanti, E., Sciunnach, D., 1997. Early carboniferous onset of gondwanian glaciation and neo-tethyan rifting in southern tibet. Earth Planet Sci. Lett. 148, 359–365.
Geske, A., Zorlu, J., Richter, D.K., Buhl, D., Niedermayr, A., Immenhauser, A., 2012. Impact of Diagenesis and Low Grademetamorphosis on Isotope (δ^{26}Mg, δ^{13}C, δ^{18}O and 87Sr/86Sr) and Elemental (Ca,Mg,Mn, Fe and Sr) Signatures of Triassic Sabkha Dolomites.
Gianolla, P., Andreetta, R., Furin, S., Furlanis, S., Riva, A., 2008. Geology of the Dolomites. Nomination of the Dolomites for Inscription on the World Natural Heritage List Unesco. Artimedia, Trento, Italy, pp. 3–77.
Gindre-Chanu, L., Borrelli, M., Caruso, A., Critelli, S., Perri, E., 2020. Carbonate/evaporitic sedimentation during the Messinian salinity crisis in active accretionary wedge basins of the northern Calabria, southern Italy. Mar. Petrol. Geol. 112, 104066.
Golonka, J., 2004. Plate tectonic evolution of the southern margin of Eurasia in the Mesozoic and Cenozoic. Tectonophysics 381, 235–273.
Grandić, S., Biancone, M., Samarzija, J., Samaržija, J., Samarzija, J., 2002. Geophysical and stratigraphic evidence of the Adriatic Triassic rift structures. Mem. della Soc. Geol. Ital. 57, 315–325.
Grandić, S., Kratkoviæ, I., Baliæ, D., 2013. Peri-Adriatic platforms Proximal Talus reservoir potential (part 1). Nafta 64, 147–160.
Granot, R., 2016. Palaeozoic oceanic crust preserved beneath the Eastern Mediterranean. Nat. Geosci. 9, 701–705.
Gregg, J.M., Sibley, D.F., 1984. Epigenetic dolomitization and the origin of xenotopic dolomite texture. J. Sediment. Res. 54, 907–931.
Gretter, N., Ronchi, A., Langone, A., Perotti, C.R., 2013. The transition between the two major Permian tectonostratigraphic cycles in the central Southern Alps: results from facies analysis and U/Pb geochronology. Int. J. Earth Sci. 102, 1181–1202.
Haq, B.U., Hardenbol, J., Vail, P.R., 1988. Mesozoic and Cenozoic chronostratigraphy and cycles of sea-level change. In: Wilgus, C.K., Hastings, B.S., Kendall, C., Posamentier, H.W., Ross, C.A., Van Wagoner, J.C. (Eds.), Sea Level Changes-An Integrated Approach, vol. 42. SEPM Special Publication, pp. 71–108.
Hardie, L.A., 1967. The Gypsum–anhydrite equilibrium at one atmosphere pressure. Am. Mineral. 52, 171–199.
Hardie, L.A., Lowenstein, T.K., Spencer, R.J., 1985. The problem of distinguishing between primary and secondary features in evaporites. In: 6th International Symposium on Salt, 1, pp. 11–39.
Harris, P.M., Purkis, S., 2019. Impact of facies and diagenetic variability on permeability and fluid flow in an oolitic grainstone—pleistocene Miami Oolite. Depositional Record 6, 459–470.
Iannace, A., Zamparelli, V., 2002. Upper Triassic platform margin biofacies and the paleogeography of southern Apennines. Palaeogeogr. Palaeoclimatol. Palaeoecol. 179 (1), 1–18.
Iannace, A., Boni, M., Zamparelli, V., 1995. The middle-upper Triassic of the San Donato Unit Auct. (northern Calabria): stratigraphy, paleogeography and tectonic implications. Riv. Ital. Paleontol. Stratigr. 101 (3), 301–324.
Iannace, A., Parente, M., Zamparelli, V., 2005. The Upper Triassic platform margin facies of Southern Apennines and their Jurassic fate: state of the art. Bollettino Società Geologica Italiana 124, 203–214.
Ietto, A., Perri, E., Ietto, F., Rende, L., 1995. The sequence of mount cocuzzo (catena costiera, Calabria) in the dolomitic trias of southern Apeninnes. Boll. Soc. Geol. Ital. 114 (1), 215–244.
Jowett, E.C., Cathles, L.M., Davis, B.W., 1993. Predicting the depths of gypsum dehydration in evaporitic sedimentary basins. AAPG (Am. Assoc. Pet. Geol.) Bull. 77, 402–413.
Kamberis, E., Kokinou, E., Koci, F., Lioni, K., Alves, T.M., Velaj, T., 2022. Triassic evaporites and the structural architecture of the External Hellenides and Albanides (SE Europe): controls on the petroleum and geoenergy systems of Greece and Albania. Int. J. Earth Sci. 111 (3), 789–821.
Karakitsios, V., Rigakis, N., 2007. Evolution and petroleum potential of western Greece. J. Petrol. Geol. 30 (3), 197–218.
Koch, G., 2020. Palynology and Palynostratigraphy of Sub- and Surface Triassic, Eastern Adriatic, Croatia: Aspects of Palaeoclimate, Geodynamics and Halokinetic Facies. LAP Lambert Academic Publishing, p. 232.
Korte, C., Kozur, H.W., Veizer, J., 2005. δ^{13}C and δ^{18}O values of Triassic brachiopods and carbonate rocks as proxies for coeval seawater and paleotemperature. Paleogeogr. Paleoclim. Paleoecol. 226, 287–306.
Kupecz, J.A., Land, L.S., Purser, B., Tucker, M., Zenger, D., 1994. Progressive recrystallization and stabilization of early-stage dolomite: lower Ordovician Ellenburger Group, west Texas. In: Purser, B., Tucker, M., Zenger, D. (Eds.), Dolomites: A Volume in Honour of Dolomieu, vol. 21. International Association of Sedimentologists Special Publication, pp. 255–279.
Land, L.S., Hoops, G.K., 1973. Sodium in carbonate sediments and rocks: a possible index to the salinity of diagenetic solutions. Jounal of Sedimentary Petrology 43 (3), 614–617.
Laubscher, H., Bernoulli, D., 1977. Mediterranean and Tethys. In: Nairn, A.E.M., Kanes, W.H., Stehli, F.G. (Eds.), The Ocean Basins and Margins. Plenum Publ. Comp. 4, New York, pp. 1–28.
Lindquist, S.J., 1999. Petroleum systems of the Po Basin Province of Northern Italy and the Northern Adriatic Sea: Porto Garibaldi (Biogenic), Meride/Riva di Solto (Thermal), and Marnoso Arenacea (Thermal), vol. 99. USGS Open-File Report.
Lipparini, L., D'Ambrosio, A., Trippetta, F., Bigi, S., Derks, J.F., Bambridge, V.R., Cassola, T., 2021. A new regional petroleum systems model for Central Italy and the central adriatic sea supported by basin modelling and an analysis of hydrocarbon occurrences. J. Petrol. Geol. 44, 461–485.
Lugli, S., 2001. Timing of post-depositional events in the Burano formation of the secchia valley (upper triassic, northern Apennines), clues from gypsumanhydrite transitions and carbonate metasomatism. Sediment. Geol. 140, 107–122.
Lugli, S., Morteani, G., Blamart, D., 2002. Petrographic, REE, fluid inclusion and stable isotope study of magnesite from the Upper Triassic Burano Evaporites (Secchia Valley, northern Apennines): contributions from sedimentary, hydrothermal and metasomatic sources. Mineralium Deposita 37, 480–494.
Malone, M.J., Baker, P.A., Burns, S.J., 1996. Recrystallization of dolomite: an experimental study. Geochem. Cosmochim. Acta 60 (12), 2189–2207.
Manaa, A.A., Aref, M.A., 2022. Microbial mats and evaporite facies variation in a supralittoral, ephemeral lake, Red Sea coast, Saudi Arabia. Facies 68, 3.
Manatschal, G., Bernoulli, D., 1998. Rifting and early evolution of ancient ocean basins: the record of the Mesozoic Tethys and of the Galicia-Newfoundland margins. Mar. Geophys. Res. 20, 371–381.
Martinis, B., Pieri, M., 1964. Alcune notizie sulla formazione evaporitica dell'Italia centrale e meridionale. Memorie Societa Geologica Italiana 4, 649–678.
Masetti, D., Fantoni, R., Romano, R., Sartorio, D., Trevisani, E., 2012. Tectonostratigraphic evolution of the Jurassic extensional basins of the eastern southern Alps and Adriatic foreland based on an integrated study of surface and subsurface data. AAPG (Am. Assoc. Pet. Geol.) Bull. 96, 2065–2089.
Mastandrea, A., Perri, E., Neri, C., Russo, F., 2003. Conodont biostratigraphy of the norian-rhaetian deposits in the northern Calabria: the valle corvino and grisolia sections. Boll. Soc. Paleont. Ital. 42, 173–182.

Mastandrea, A., Perri, E., Russo, F., Spadafora, A., Tucker, M., 2006. Microbial primary dolomite from a Norian carbonate platform: northern Calabria, southern Italy. Sedimentology 53, 465–480.
Meister, P., McKenzie, J.A., Bernasconi, S.M., Brack, P., 2013. Dolomite formation in the shallow seas of the Alpine Triassic. Sedimentology 60, 270–291.
Montanez, I.P., Read, J.F., 1992. Eustatic control on early dolomitization of cyclic peritidal carbonates: evidence from the early ordovician upper knox group, appalachians. Geol. Soc. Am. Bull. 104, 872–886.
Morsilli, M., 2016. Sintesi delle conoscenze geologiche e stratigrafiche del promontorio del Gargano, Geologi e Territorio. Ordine Regionale dei Geologi Puglia 2, 15–30.
Morsilli, M., Hairabian, A., Borgomano, J., Nardon, S., Adams, E.W., Bracco Gärtner, G. L., 2017. The Apulia carbonate platform in the Gargano promontory (upper jurassic to eocene - southern Italy). Am. Assoc. Petrol. Geol. Bull. 4, 523–531.
Passeri, L., 1975. L'ambiente deposizionale della formazione evaporitica nel quadro della paleogeografia del Norico tosco-umbro-marchigiano. Boll. Soc. Geol. It. 94, 231–268.
Patacca, E., Scandone, P., Di Luzio, E., Cavinato, G.P., Parotto, M., 2008. Structural architecture of the central Apennines: interpretation of the CROP 11 seismic profile from the Adriatic coast to the orographic divide. Tectonics 27, TC300.
Pedley, H.M., Grasso, M., 1993. Controls on faunal and sediment cyclicity within the tripoli and calcare di Base basins (late Miocene) of central sicily. Palaeogeogr. Palaeoclimatol. Palaeoecol. 105, 337–360.
Pemberton, S.G., Wightman, D.M., 1992. Ichnological characteristics of brackish water deposits. In: Pemberton, S.G. (Ed.), Applications of Ichnology to Petroleum Exploration, SEPM Core Workshop 17, pp. 141–167.
Perri, E., Borrelli, M., Bernasconi, M.P., Gindre-Chanu, L., Spadafora, A., Critelli, S., 2019. Microbial-dominated carbonate depositional systems: a biosedimentary and stratigraphic reconstruction in the Late Triassic of Western Tethys (northern Calabria, Italy). Facies 65, 31.
Perri, E., Borrelli, M., Spadafora, A., Critelli, S., 2017. The role of microbialitic facies in the micro- and nano-pore system of dolomitized carbonate platforms (Upper Triassic of southern Italy). Mar. Petrol. Geol. 88, 1–17.
Perri, E., Tucker, M., 2007. Bacterial fossils and microbial dolomite in Triassic stromatolites. Geology 35, 207–210.
Perri, E., Tucker, M.E., Mawson, M., 2013. Biotic and abiotic processes in the formation and diagenesis of Permian dolomitic stromatolites (Zechstein, NE England). J. Sediment. Res. 83, 20.
Perri, E., Tucker, M.E., Słowakiewicz, M., Whitaker, F., Bowen, L., Perrotta, I.D., 2018. Carbonate and silicate biomineralization in a hypersaline microbial mat (Mesaieed sabkha, Qatar): roles of bacteria, extracellular polymeric substances and viruses. Sedimentology 65, 1213–1245.
Piccardi, L., Sani, F., Moratti, G., Cunningham, D., Vittori, E., 2011. Present-day geodynamics of the circum-Adriatic region: an overview. J. Geodyn. 51, 81–89.
Rigo, M., Preto, N., Roghi, G., Tateo, F., Mietto, P., 2007. A rise in the carbonate compensation depth of western Tethys in the carnian: deep-water evidence for the carnian pluvial event. Palaeogeogr. Palaeoclimatol. Palaeoecol. 246, 188–205.
Ronchi, A., Santi, G., Marchetti, L., Bernardi, M., Gianolla, P., 2018. First report on swimming trace fossils of fish from the upper permian and lower triassic of the dolomites (Italy). Ann. Soc. Geol. Pol. 88, 111–125.
Rouchy, J.M., Caruso, A., 2006. The Messinian salinity crisis in the Mediterranean basin: a reassessment of the data and an integrated scenario. Sediment. Geol. 188, 35–67.
Russo, F., Gautret, P., Mastandrea, A., Perri, E., 2006. Syndepositional cements associated with nannofossils in the Marmolada Massif: evidences of microbially mediated primary marine cements? (Middle Triassic, Dolomites, Italy). Sediment. Geol. 185 (3–4), 267–275.
Sánchez-Román, M., McKenzie, J.A., de Luca Rebello Wagner, A., Romanek, C.S., Sánchez-Navas, A., Vasconcelos, C., 2011. Experimentally determined biomediated Sr partition coefficient for dolomite: significance and implication for natural dolomite. Geochem. Cosmochim. Acta 75, 887–904.
Santantonio, M., Scrocca, D., Lipparini, L., 2013. The ombrina-rospo plateau (apulian platform): evolution of a carbonate platform and its margins during the jurassic and cretaceous. Mar. Petrol. Geol. 42, 4–29.
Scandone, P., 1975. Triassic seaways and the jurassic Tethys Ocean in the central mediterranean area. Nature 256, 117–119.
Schettino, A., Turco, E., 2006. Plate kinematics of the western Mediterranean region during the Oligocene and early Miocene. Geophys. J. Int. 166, 1398–1423.
Schreiber, B.C., 1982. Evaporites. Geotimes 27, 31.
Schreiber, B.C., El Tabakh, M., 2000. Deposition and early alteration of evaporites. Sedimentology 47, 215–238.
Scisciani, V., Calamita, F., 2009. Active intraplate deformation within Adria: examples from the adriatic region. Tectonophysics 476 (1–2), 57–72.
Scisciani, V., Esestime, P., 2017. The triassic evaporites in the evolution of the Adriatic Basin. In: Soto, J.I., Flinch, J.F., Tari, G. (Eds.), Permo-Triassic Salt Provinces of Europe, North Africa and Atlantic Margins: Tectonics and Hydrocarbon Potential. Elsevier, Amsterdam, pp. 499–516.
Scotese, C.R., Schettino, A., 2017. Late permian-early jurassic paleogeography of western Tethys and the world. In: Soto, J.I., Flinch, J.F., Tari, G. (Eds.), Permo-Triassic Salt Provinces of Europe, North Africa and Atlantic Margins: Tectonics and Hydrocarbon Potential. Elsevier, Amsterdam, pp. 57–95.
Scrocca, D., Doglioni, C., Innocente, F., Manetti, P., Mazzotti, A., Bertelli, L., Burni, L., D'Offizi, S., 2003. CROP Atlas: seismic reflection profiles of the Italian crust. Mem. Descr.lla Carta Geol. Italia 62, 193.
Sellwood, B.W., Valdes, P.J., 2006. Mesozoic climates: general circulation models and the rock record. Sediment. Geol. 190, 269–287.
Shearman, D.J., 1985. Syndepositional and late diagenetic alteration of primary gypsum to anhydrite. In: Schreiber, B.C., Harner, L. (Eds.), 6th Int. Symposium on Salt 1. Salt institute, pp. 41–50.
SibIey, D.F., 1982. The origin of common do!omite fabrics. J. Sediment. Petrol. 52, 1987.
Sibley, D.F., Gregg, J.M., 1987. Classification of dolomite rock textures. J. Sediment. Res. 57, 967–975.
Slowakiewicz, M., Perri, E., Tucker, M.E., 2016. Micro-and nanopores in tight Zechstein 2 carbonate facies from the southern Permian Basin, NW Europe. J. Petrol. Geol. 39 (2), 149–168.
Stampfli, G.M., Hochard, C., Verard, C., Wilhem, C., von Raumer, J., 2013. The formation of Pangea. Tectonophysics 593, 1–19.
Stefani, M., Furin, S., Gianolla, P., 2010. The changing climate framework and depositional dynamics of Triassic carbonate platforms from the Dolomites. Palaeogeogr. Palaeoclimatol. Palaeoecol. 290, 43–57.
Tamas, M., Baldi-beke, M., Kazmer, I.D., Von Eytten, H., 2008. Calcareous nannofossil age constraints on Miocene flysh sedimentation in the Outer Dinarides (Slovenia, Croatia, Bosnia-Herzegovina and Montenegro). In: Siegesmund, S., Fugenschuh, B., Froitzheim, N. (Eds.), Tectonic Aspects of the Alpine-Dinaride-Carpathian System, vol. 298. Geological Society London, pp. 335–363.
Tari, V., 2002. Evolution of the Northern and Western Dinarides: a Tectonostratigraphic Approach, vol. 1. EGU Stephan Mueller Special Publication Series, pp. 223–236.
Teofilo, G., Festa, V., Sabato, S., Spalluto, L., Tropeano, M., 2016. 3D modelling of the Tremiti salt diapir in the Gargano offshore (Adriatic Sea, southern Italy): constraints on the Tremiti Structure development. Italian J. Geosci. 135 (3), 474–485.
Testa, G., Lugli, S., 2000. Gypsum–anhydrite transformations in Messinian evaporites of central Tuscany (Italy). Sediment. Geol. 130, 249–268.
Tucker, M.E., Wright, V.P., 1990. Carbonate Sedimentology. Blackwell Scientific Publications, Oxford, UK.
Vai, G.B., 2001. Basement and early (Pre-Alpine) history. In: Vai, G.B., Martini, I.P. (Eds.), Anatomy of an Orogen: the Apennines and Adjacent Mediterranean Basins. Kuwler Academic Publishers, Dordrecht, The Netherlands, pp. 65–76.
Vasconcelos, C., Warthmann, R., McKenzie, J.A., Visscher, P.T., Bittermann, A.G., van Lith, Y., 2006. Lithifying microbial mats in lagoa vermelha, Brazil: modern precambrian relics? Sediment. Geol. 185, 175–183.
Veizer, J., Ala, D., Azmy, K., Bruckschen, P., Bruhn, F., Buhl, D., Carden, G., Diener, A., Ebneth, S., Goddris, Y., Jasper, T., Korte, C., Pawellek, F., Podlaha, O., Strauss, H., 1999. 87Sr/86Sr, $\delta^{13}C$ and $\delta^{18}O$ evolution of Phanerozoic seawater. Chem. Geol. 161, 59–88.
Velić, J., Malvić, T., Cvetković, M., Velić, I., 2015. Stratigraphy and petroleum geology of the Croatian part of the Adriatic Basin. J. Petrol. Geol. 38, 281–300.
Virgili, C., Cassinis, G., Broutin, J., 2006. Permian to Triassic sequences from selected continental areas of southwestern Europe. In: Lucas, S.G., Cassinis, G., Schneider, J. W. (Eds.), Non-Marine Permian Biostratigraphy and Biochronology, vol. 265. Geological Society, London, Special Publications, pp. 231–259.
Vlahović, I., Tišljar, J., Velić, I., Matičec, D., Vlahovic, I., Tisljar, J., Velic, I., Maticec, D., 2005. Evolution of the adriatic carbonate platform: palaeogeography, main events and depositional dynamics. Palaeogeogr. Palaeoclimatol. Palaeoecol. 220, 333–360.
von Raumer, J.F., Janousek, V., Stampfli, G.M., 2012. Durbachites-vaugnerites, a time-marker across the European Variscan basement. Géologie de la France 2012 (1), 178–180.
Warren, J.K., 2000. Dolomite: occurrence, evolution and economically important associations. Earth Sci. Rev. 52, 1–81.
Warren, J.K., 2006. Evaporites: Sediments, Resources and Hydrocarbons. Springer, Berlin, p. 1036.
Wheeler, C.W., Aharon, P., Ferrell, R.E., 1999. Successions of Late Cenozoic platform dolomites distinguished by texture, geochemistry, and crystal chemistry: Niue, South Pacific. J. Sediment. Res. 69 (1), 239–255.
Wrigley, R., Hodgson, N., Esestime, P., 2015. Petroleum geology and hydrocarbon potential of the Adriatic basin, offshore Croatia. J. Petrol. Geol. 38 (3), 301–316.
Zappaterra, E., 1994. Source-rock distribution model of the periadriatic region. AAPG (Am. Assoc. Pet. Geol.) Bull. 78, 333–354.
Ziegler, A.M., Hulver, M.L., Rowley, D.B., 1997. Permian world topography and climate. In: Martini, I. (Ed.), Late Glacial and Postglacial Environmental Changes: Quaternary, Carboniferous-Permian and Proterozoic. Oxford University Press, pp. 11–146.